Where top-down meets bottom-up: Cell-type specific connectivity map of the whisker system

Rault N.[1], Bergmans T.[1], Delfstra N.[1], Kleijnen BJ[1], Zeldenrust F.[1] and Celikel T.[2]

[1]Donders Institute, Radboud University, Nijmegen, The Netherlands.
[2]Georgia Institute of Technology, Atlanta, GA, USA.

Abstract - Sensorimotor computation is a closed-loop process where bottom-up information collected about the current state of the world is integrated with top-down, internally generated knowledge and task- and goal-related affordances to create an action plan. In the rodent whisker system, a canonical model of sensorimotor computation in the context of active sensing, emerging evidence suggests that neuromodulatory neurotransmitters help shape sensorimotor control of the whisker position and contribute to context-dependent changes in whisking frequency and amplitude. Since neuromodulatory neurotransmitters are mostly released from subcortical nuclei and have long-range projections that reach the rest of the central nervous system, mapping the circuits of top-down neuromodulatory control of sensorimotor nuclei will help to systematically address the mechanisms of active sensing. Therefore, taking advantage of the Allen Institute's Mouse Connectivity database, we provide an updated, cell-type specific map of the sensorimotor circuits in the mouse brain. The map includes 138 projections (54 of which were not previously reported in the literature) across 18 principal and neuromodulatory neurotransmitter-releasing nuclei of the whisker system. Performing a graph network analysis of this connectome, we identify cell-type specific hubs, sources, and sinks, provide anatomical evidence for monosynaptic inhibitory projections into all stages of the ascending pathway, and show that neuromodulatory projections improve network-wide connectivity. These results argue that beyond the modulatory chemical contributions to information processing and transfer in the whisker

system, the circuit connectivity features of the neuromodulatory networks position them as nodes of sensory and motor integration.

List of abbreviations

TG - Trigeminal Ganglion
PSV - Principal sensory nucleus
SPVO, SPVI, SPVC - spinal nucleus of the trigeminal oralis, interpolaris, caudalis
VPM - ventral posteromedial nucleus
PO - posterior complex of the thalamus
RT - Reticular Nucleus of the thalamus
bfd - barrel field of the primary somatosensory cortex
MOp - primary motor cortex
SC - Superior Colliculus
VII - Facial Motor nucleus
ZI - Zona Incerta
SI - Substantia Innominata
DR - Dorsal raphe nucleus
LC - Locus coeruleus
PPN - Pedunculopontine nucleus
VTA - Ventral tegmental area
TM - Tuberomammillary nucleus

1 Introduction

In the wild, whisking rodents are subterranean mammals that live in dark and narrow environments. They heavily rely on the rhythmic protraction and retraction of their whiskers to navigate their natural habitat. Organized as closed-loop circuits (**Kleinfeld et al., 1999**), distributed networks in the brain control whisking as an adaptive sensorimotor computation while they encode sensory information originating from the sensory periphery and compute the future position of the whiskers as an iterative process (**Voigt et al., 2008**, **Voigt et al., 2015**, **McElvain et al., 2018**).

The neural circuits that contribute to the sensory representations acquired through whisker contacts and the positional controls of whiskers were last summarized more than a decade ago **(Bosman et al., 2011)**. Building on 1) the first comprehensive sensorimotor circuit map in the whisker system (**Kleinfeld et al., 1999**), 2) the fundamental experimental work that described the lemniscal and paralemniscal ascending neural circuits (**Chial et al., 1991**, **Lu and Lin, 1992**), and 3) the descending projections originating from the motor cortex (**Ashwell, 1982**, **Hemelt and Keller, 2008**), Bosman and colleagues described the connectome between 43 nuclei contributing to the sensorimotor integration in the whisker system. In particular, 12 of the nuclei described in

their studies as well as 6 brainstem regions that release neuromodulatory transmitters showed 74 connections (**Supplemental Figure 1**, for the complete network **Supplemental Figure 4**).

In addition to the nuclei from the ascending somatosensory pathway and the motor cortex, we consider the following networks in our updated whisker system connectivity map: The facial motor nucleus (VII) , as it contains the motoneurons innervating the muscle situated in the whisker pad (**Ashwell, 1982**). The Superior Colliculus (SC), as it is targeted by connections from the trigeminal nuclei and targets VII (**Hemelt and Keller, 2008**). The reticular nucleus of the thalamus (RT) is added as the main source of inhibition of the thalamic nuclei (**Pinault et al., 1995**). The Zona Incerta (ZI) is included in the map for its role in the paralemniscal pathway (**Urbain and Deschênes, 2007a**) and its somatotopic map representation of whiskers (**Nicolelis et al., 1992**). The neuromodulator-releasing nuclei are added to the map as one of the goals of the study is to analyze the structure of the network with and without these nuclei, in order to try to determine if they could be qualified as hubs in the whisker system.

Over the last decade, new experimental studies provided direct evidence that the network connectivity along the whisker system is more expansive than previously shown. For example, a study by **Minju Jeong et al., 2016**, focusing on the motor nuclei in the mouse, in particular MOp, revealed projections to PO and VPM in the thalamus, as well as to the contralateral PSV, SPV, and VTA. This latter connection and the monosynaptic MOp projections to PPN and SPVi were independently confirmed (**Rodrigo Muñoz-Castañeda et al., 2021**). In parallel, direct monosynaptic projections originating from bfd and targeting TM, RT, and ZI (**Izabela M. Zakiewicz et al., 2014**), ZI projections to VII (**Takatoh et al., 2021**), VII innervation of SPVi (**Bellavance et al., 2017**), VPM to MOp connections (**Bryan M. Hooks et al., 2013**) and bidirectional communication between MOp and RT were shown (**Yang et al., (2022)**). Moreover, newly identified connections were not only found among primarily sensory and motor nuclei. **Jonas A. Hosp et al., 2011** identified a projection between VTA and MOp, showing the contribution of dopaminergic connections originating from VTA in motor skill learning. Other studies showed that VTA serves as a hub of divergence with projections to SI, LC, DR, RT (**Anna I. Dunigan et al., 2021**), and bfd (**Anna Aransay et al., 2015**), all critical for the information processing in the whisker system. Finally, the novel discoveries along the neuromodulatory circuits and their integration with nuclei in the whisker system are not limited to the dopaminergic system. Monosynaptic cholinergic projections to RT (**Guela Sokhadze et al., 2018**), SI projections to ZI (**Zhou et al., 2018**), ZI projections to VTA (**An et al., (2021)**), reciprocal connections between PO and SC (**Benavidez et al., 2021**), SI projections to PSV, VTA, VPM, SI (**Benavidez et al., 2021**) and DR (**Benavidez et al., 2021**, **Dorocic et al., (2014)**) all provide anatomical evidence for neuromodulatory contributions to sensorimotor control.

The newly found connections mentioned above require an update of the previously drawn connectivity map of the rodent whisker system. Here we provide the third-generation connectivity map using data made publically available by the Allen Brain Institute (**Oh, S.W. et al., 2014**) and an open-source toolbox we developed to systematically analyze the data (https://github.com/DepartmentofNeurophysiology/NeuralNet-ABC). By analyzing 732 anterograde tracing experiments performed in 95 wild-type and transgenic lines, we determine the connectivity along the ascending, descending, and neuromodulator pathways. We show that the sensorimotor circuits in the whisker system includes 162 projections; 54 of these projections had not been described in the literature previously. By performing graph network analysis we further identify cell-type specific hubs, sources, and sinks in this connectome, and finally, show that neuromodulatory projections improve the network-wide connectivity.

2 Materials & Methods

2.1 Experimental pipeline

All experimental data are available online (https://connectivity.brain-map.org/) and experimental procedures have been detailed by the Allen Brain Institute before (**Oh, S.W. et al., 2014**). In short, genetically encoded fluorescent proteins were expressed in anatomically targeted regions using cell-type specific or non-specific promoters in transgenic and wild-type mice. The resulting anterograde projection labeling was visualized using serial two-photon tomography. The data were projected onto a 3D normal brain built upon a volumetric average template from 1,675 wild-type mice with 10 μm isotropic voxel resolution. The 3D reference brain was then parcellated into 43 isocortical areas, 329 subcortical gray matters structures, 81 fiber tracts, and 8 ventricular structures for each hemisphere to identify the main anatomical origin and target areas based on a standard atlas (**Wang et al., 2020**). For each structure, four variables were extracted: the volume, the intensity, the density, and the energy. The volume represents the volume of tracer solution in mm^3 present in a brain structure; the intensity is the sum of the brightness of every pixel in a given structure (the tracer producing a fluorescent reaction); the density is the number of pixels considered as expressing the gene divided by the total amount of pixels present in the structure, and the energy is the sum of pixel intensities divided by the number of pixels in the structure. The results were stored in a JSON format containing the list of structures with their associated extracted variables. To build our connectivity matrices, we first downloaded the data using Allen Brain Institute's API (**Figure 1**), and identified experiments that targeted 18 target nuclei which have been experimentally identified as a part of the sensorimotor circuits in the rodent brain (**Supplemental Figure 1**). Each experiment was saved in a JSON file containing a list of structures (723 per hemisphere) and the measures of the projection volume, intensity, density, and energy. Next, we grouped the experiments per transgenic line and

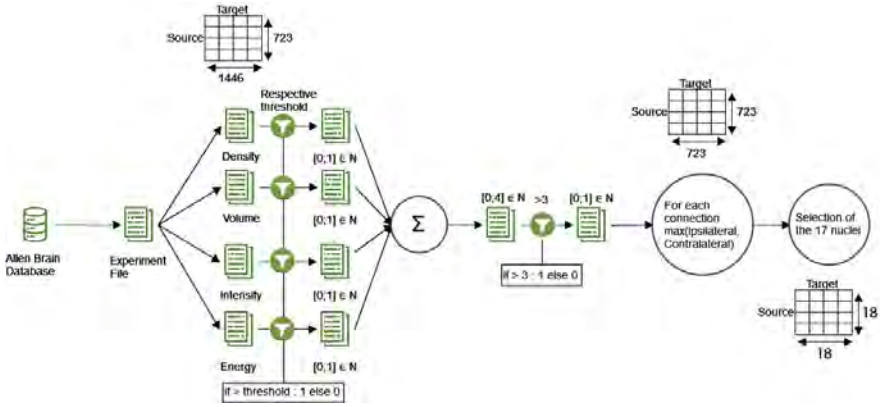

Fig. 1 The data processing pipeline. For each transgenic line, the data were downloaded from the Allen Brain database. Each experiment file was split into 4 matrices of size 723x1446, one per variable (density, volume, intensity, and energy). A threshold specific to each variable (see Connectivity Validation) was applied and 4 matrices with values of either zero or one were retrieved. These matrices were summed and a threshold equal to 4 was applied, so that only the connections that satisfied the conditions on all 4 variables remained. This way, a matrix composed of zeros and ones was obtained. Due to the sparse nature of contralateral hemispheric projections, which will increase the false negative rate, the connectomes across the hemispheres were merged by selecting the highest value. From the resulting matrix of size 723x723, we retrieved the connections for the nuclei of interest (see Supplemental Figure 1.b and 1.c). This resulted in a binary connectivity matrix with 324 (18x18) possible edges.

projected the data from each experiment onto a 723x1446 matrix (723 structures for each hemisphere), with the sources of the experiments as rows and the structures receiving the connections as columns (**Figure 1**).

2.2 Transgenic categorization

Transgenic lines were considered "excitatory" if presented as such in the literature or if the marked cells were glutamatergic, i.e. for example expressed glutamate or vesicular glutamate transporters and other proteins necessary for glutamatergic signaling. "Inhibitory" cells were classified as cells expressing Gamma-Aminobutyric Acid (GABA), glycine neurotransmitters, or other proteins related to inhibitory signaling, such as GABA receptors. Transgenic lines were classified as "uncategorized" if marked cells expressed both excitatory and inhibitory proteins, or if they expressed neither (e.g., dopamine, adrenaline, serotonin, or other neuromodulatory proteins with no direct excitatory or inhibitory effect). See **Supplemental Table 1** for the list and the corresponding citations.

2.3 Connectivity validation

To validate the connections identified in the connectivity matrices derived from the Allen Brain Institute's experiments, we compared them to a subset (N=34)

of connections previously reported by Bosman et al. (2011). For each variable, we determined a variable-specific threshold by systematically increasing the threshold until one of the 34 reference connections was no longer detected in wild-type experiments. The last value for which we found 100% of true positives was considered the correct threshold. This process yielded four distinct thresholds, which were applied to each transgenic line (density threshold: 0.0002416 (a.u.), intensity threshold: 110.8 (a.u.), energy threshold: 0.00668 (a.u.), volume threshold: 0.01559 (in mm^3)).

A connection was considered valid only if it appeared on each variable-specific matrix after threshold application. This approach ensured that we retained previously known connections while avoiding assumptions about the underlying connectivity that might have arisen from minimizing false positives. By focusing solely on true positives, we did not impose any preconceived notions about the pattern of connectivity between different nuclei. Cross-validating our connections with the four available variables minimized the likelihood of false negatives. As an additional safeguard, we verified that the genes marked by the transgenic lines in the Allen Brain Institute's experiments were indeed expressed in the targeted structure using the transgenic characterization tool available on the Allen Brain Institute's website. Applying these thresholds resulted in four connectivity matrices: one for the wild type (Figure 2.a and 2.b) and one for each transgenic characterization (excitatory, inhibitory, or uncategorized, respectively: Figure 3.a, 3.b, and 3.c) and compiled into connectivity maps (Figure 4, Supplemental Figure 2 and 3). To corroborate the connections, calculations were repeated across animal lines. New connections were only validated by experiments on at least two different transgenic lines (Figure 5). Finally, we constructed a summary map that included previously established and newly discovered connections (Figure 8). For anatomical validation of the identified connections, we superimposed the results from the 2-photon imaging experiments onto a mean model of the mouse brain. The two images for each connection were manually aligned using fiducial markers such as the hippocampus or the outline of the brain. Limitations of this approach are discussed in the text.

2.4 Network analysis

Based on the obtained connectivity maps, we analyzed the network properties of neuromodulator-releasing nuclei and their contribution to the overall connectivity of the sensorimotor circuit. To assess the small-world nature of our network, we compared our summary graph to an Erdos-Renyi (ER) graph. First, we determined the total number of connections in our summary map and calculated the probability of a connection. We then constructed an ER graph with the same number of edges, nodes, and connection probability. Using the GRETNA toolbox (**Jinhui Wang et al., 2015**), we computed the clustering coefficient and the shortest path for both the original and the ER graph. According to Watts and Strogatz (**1998**), a small-world network exhibits higher clustering values and a lower shortest path length compared to

ordered and random networks. We therefore considered our summary network to be a small-world network if its clustering coefficient was higher than that of the ER graph and its average shortest path was lower than that of the ER graph.

In addition to the ER network, we constructed a summary graph without the neuromodulator-releasing nuclei. We then computed the nodal clustering coefficient, the nodal shortest path, the degree centrality, the nodal efficiency, the nodal local efficiency, and the betweenness centrality for both networks. To determine whether the neuromodulator-releasing nuclei had an impact on the network structure, we compared the distributions of these values using a permutation test with 10,000 permutations.

Finally, we assessed the divergence ratio of each nucleus presented in the large network (57x57, **Supplemental Figure 4**). To do that, we first computed the out-degree as the sum of output and the in-degree as the sum of input for each node.

The ranked order of out-degree was used to visualize the directed nature of the projections (**Figure 6**). We subsequently computed the divergence ratio for each node with the following equation:

$$\text{ratio}_{\text{divergence}} = \frac{(\text{degree}_{\text{out}} - \text{degree}_{\text{in}})}{(\text{degree}_{\text{out}} + \text{degree}_{\text{in}})}$$

The results from this equation ranged between -1 for convergent nodes and 1 for divergent nodes (see **Figure 7**). A node with a $\text{ratio}_{\text{divergence}}$ of 0 is considered balanced as it possesses the same amount of outputs as inputs. To ensure that nuclei were of divergent or convergent nature, we fitted a Gaussian centered around 0, which corresponds to taking the mean and the standard deviation of the balanced nodes. We then applied a confidence interval of 2 standard deviations around the mean.

3 Results

We analyzed data from 162 experiments on wild-type mice and 570 experiments on 94 different transgenic lines. The 18-nuclei sub-network described in the introduction was targeted by 52 experiments on wild-type mice and 159 experiments on 52 different transgenic lines focused on these 18 nuclei (**Supplemental Figure 1**). Out of the $18 \times 18 = 324$ possible connections for each type of mice, 237 connections were identified in the wild-type strain. Experiments on the transgenic lines revealed 151 excitatory connections, 198 inhibitory connections, and 211 uncategorized connections exhibiting values above 0 without threshold application. Among these 797 connections, 48.31% (i.e., 385 projections) met the criteria for anatomical connections (refer to Materials and Methods for details). For the 18-nuclei sub-network, **Bosman et al., 2011** observed 74 connections (**Supplemental Figure 1.b, 1.c**). Our study identified 142 connections in the wild type (**Figure 2.a, 2.b**) and 243 connections in the 49 transgenic lines examined for these structures and exhibiting connections. The identified connections are distributed across

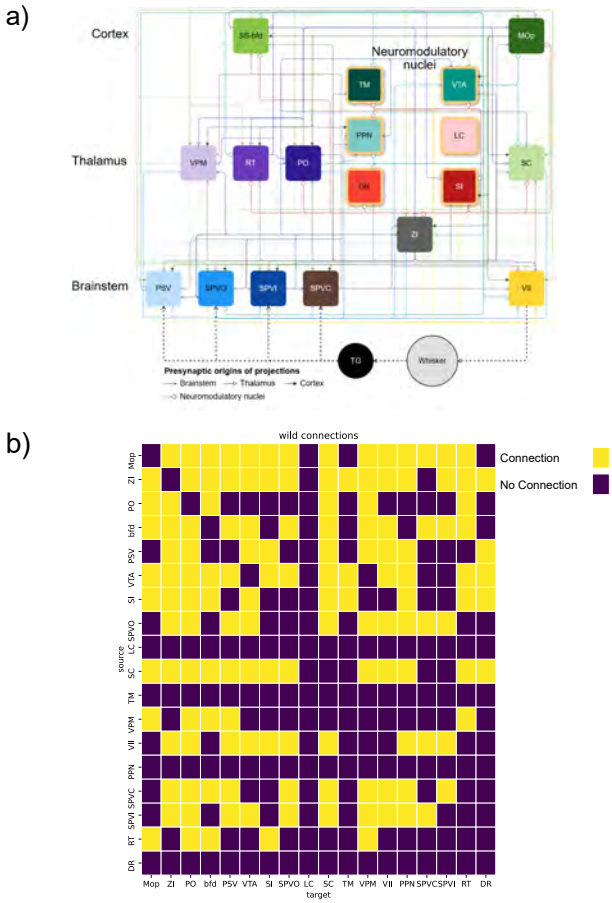

Fig. 2 Sensorimotor connectivity map of the whisker system in wild-type mice. **a)** Connectivity map across 18 nuclei with 142 connections computed from wild-type experiments in the Allen Brain database. A dashed line represents a flow of information outside of the central nervous system. The neuromodulatory structures are represented with yellow borders. **b**) Binary representation of the connectivity matrix. LC, TM, PPN, and DR were not targeted in wild-type animals, thus their projections to the rest of the network are not shown. See Figure 3 for the results from transgenic animals and Figure 8 for the compiled connectome.

the different cell-type-specific connectivity maps. Among these connections, 61 are excitatory (**Figure 3.a; Supplemental Figure 2)**, 87 are inhibitory (**Figure 3.b; Figure 4**), and 95 are uncategorized (**Figure 3.c; Supplemental Figure 3**), with 29 of these not appearing on either excitatory or inhibitory connectivity maps (**Figure 3.d**). There is a 27% overlap between excitatory connections and inhibitory connections, a 27% overlap between inhibitory connections and uncategorized connections, and a 29% overlap between excitatory connections and uncategorized connections.

Among the structures presented in this study, the tuberomammillary nucleus, the locus coeruleus, and the oral part of the spinal nucleus have

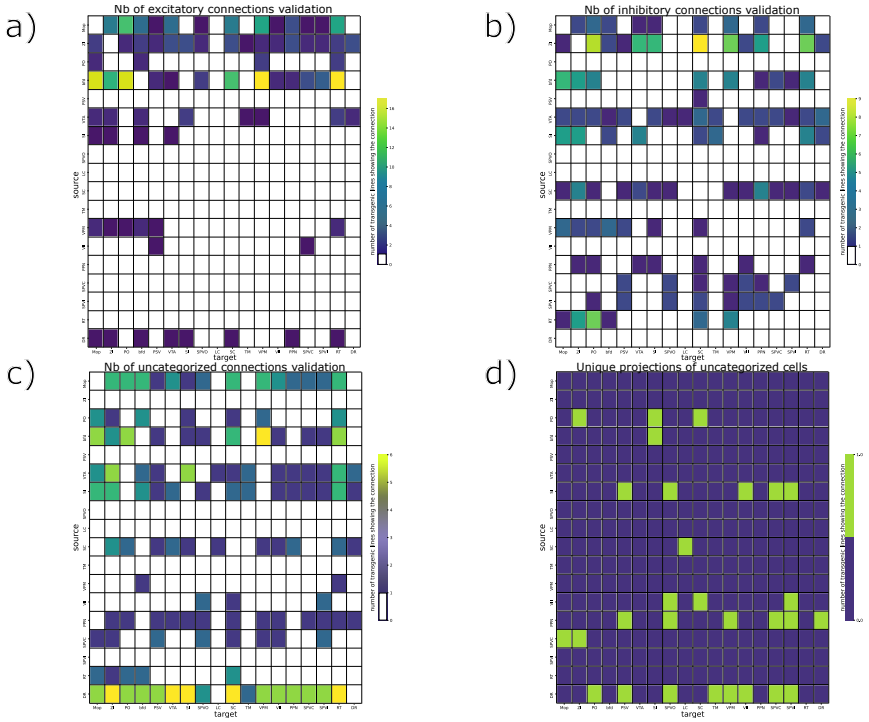

Fig. 3 Number of confirmations per cell-type. Vertical axes represent the source, and the horizontal ones the target. In a-c, the colors represent the number of transgenic lines confirming the connection. **a)** Experiments on excitatory transgenic lines unveiled 61 connections, mostly originating from the cortex and the zona incerta. **b)** A total of 87 connections were discovered in inhibitory transgenic lines. **c)** Experiments on uncategorized transgenic lines unveiled 95 connections. Note the divergence of projections originating from VTA, SI, PPN, and DR, all neuromodulatory neurotransmitter-releasing nuclei. **d)** A binary representation of unique projections in cell classes that either express both excitatory and inhibitory markers or neither. A total of 29 connections were identified, none of which appeared in excitatory or inhibitory connectomes of the sensorimotor circuit.

not been targeted by experiments in the Allen Brain database, resulting in a lack of connectivity data for these structures. Additionally, on the wild-type map, connectivity data is not available for the tuberomammillary nucleus, the pedunculopontine nucleus, the locus coeruleus, and the dorsal nucleus raphe.

In the next sections, we will discuss the connections originating from each of the 18 nuclei, validated by our methods.

3.1 Trigeminal nuclei

The information originating upon whisker contact with a surface propagates along the brainstem, the thalamus, and the primary somatosensory cortex while making closed-loop connections with the motor system (**Kleinfeld et al., 1999**). This information is not solely transmitted via excitatory connections, as inhibition is observed early in the sensory pathway (**Kleinfeld et al.,**

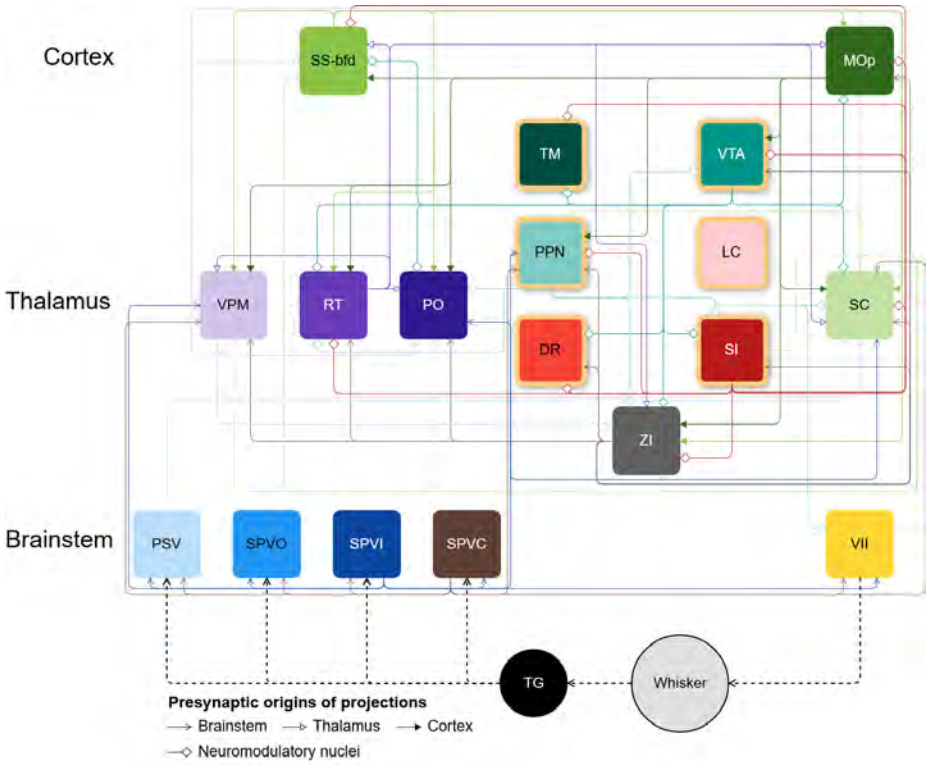

Fig. 4 The connectome of the inhibitory projections in the mouse whisker system. The connectivity map includes 87 connections. A dashed line represents the flow of information outside of the central nervous system. The nodes with yellow borders are neuromodulatory structures.

1999). In line with this, our findings reveal the presence of inhibitory presynaptic cells in PSV, SPVi, and SPVc. This suggests that both inhibitory and excitatory activity play a role in processing tactile information as early as the brainstem (**Figure 5**).

Our findings reveal an inhibitory connection originating from SPVi targeting SC. The inhibitory nature of synaptic projections from SPVi to trigeminal nuclei and VII suggests an inhibitory control of touch processing already at the brainstem level. Moreover, SPVi projections to PO and VPM, further emphasize the brainstem's role in whisker information processing. The presence of this ascending inhibition implies that SPVi not only relays information but also filters it. Additionally, SPVi projects to PPN, hinting at a potential role in modulating cholinergic neurons. The connections to PO, SPVo, and SPVc were validated in at least two animal lines.

SPVi is not the only structure that targets cholinergic neurons. We demonstrate that inhibitory presynaptic cells in the trigeminal complex target other trigeminal nuclei and establish long-range connections to low-level structures of the motor pathway and acetylcholine-releasing nucleus. As described by

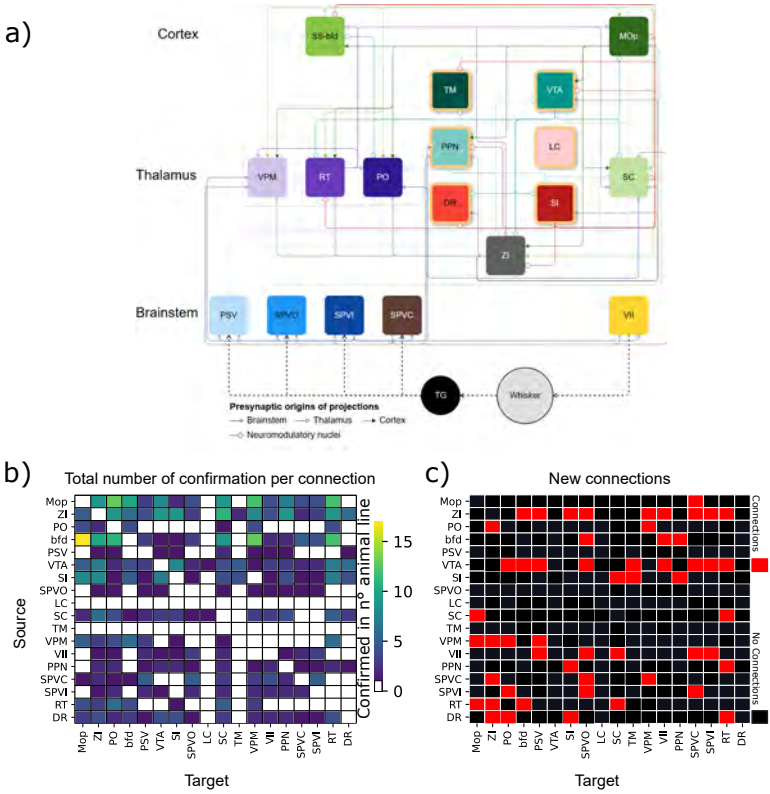

Fig. 5 Newly discovered monosynaptic projections across the sensorimotor map of the mouse whisker system. a) A graphical representation of the connectome. A dashed line represents the flow of information outside of the central nervous system. The neuromodulatory structures are represented with yellow borders. **b)** 189 connections were identified in the experiments from the Allen Brain database. 134 of these connections were confirmed in at least two mouse lines and have been included in the final connectome (Figure 8). The vertical axis represents the source of the connection, and the horizontal axis the target. The color scale indicates the number of mouse lines that confirm the presence of the connections. **c)** These 54 (out of 134) projections have not been previously described in the literature to the best of our knowledge.

Esmaeili et al. (2020), acetylcholine is thought to play a role in associating a whisker stimulus with a reward expectation. Through a direct connection from the trigeminal nuclei to PPN, low-level structures of the ascending somatosensory pathways can modulate cholinergic reward signals.

Our findings showed that SPVc inhibits the trigeminal nuclei, PPN, SC, VII, and VPM. Unclassified connections were found targeting ZI. Connections toward ZI, SPVo, and VPM were confirmed in at least two animal lines. These findings corroborate previous observations by **Jacquin et al. (1990)**, who demonstrated dense intersubnuclear connections in the rat's trigeminal complex. Finally, the presence of inhibition in the trigeminal nuclei suggests a significant role for this node in filtering information in these early sensory structures.

3.2 Thalamus

Traditionally, thalamic nuclei of the somatosensory system are considered as relay nuclei that contribute to the spatiotemporal representation of touch (**Ahissar and Arieli, 2001, Azarfar et al., 2018**). It is widely accepted that feed-forward excitatory projections originating from the ventral posteromedial (VPM) and posterior medial (PoM) nuclei, targeting the barrel field cortical columns and septa, respectively, constitute the primary pathway for information flow (**Kleinfeld et al., 1999**). However, our surprising findings argue that these projections not only include feed-forward excitation but also incorporate feed-forward inhibition. This finding has significant implications, as it reshapes our understanding of intrathalamic communication between the VPM and PoM nuclei.

Long-range connections from VPM originate from both excitatory and inhibitory cells. In addition to directly exciting bfd, MOp, PO, and RT, VPM sends top-down excitatory projections to PSV. Direct inhibition (Supplemental Figures 7 and 34) of MOp, bfd, SC, ZI, RT, and PO has been demonstrated to originate from VPM. Uncategorized connections originating from VPM target both bfd and RT. The connections originating in VPM and targeting MOp, ZI, PO, and PSV were found in at least two different animal lines. These findings suggest that VPM plays a complex role in shaping sensory information flow and sensorimotor transformations within the thalamus.

PO exhibits excitatory connections with RT, VPM, bfd, and MOp. Uncategorized connections were also identified between ZI and RT. The connections targeting VPM and ZI, observed in at least two animal lines, were not previously reported.

Inhibitory connections originating from RT target MOp, bfd, SC, VPM, PO, and ZI. The connections toward MOp, ZI, and bfd were validated by at least two animal lines.

While inhibition of the somatosensory thalamus is generally attributed to ZI and RT activity **(Barthó et al., 2002)**, our findings reveal the presence of presynaptic inhibitory neurons in VPM, specifically connecting to PO. Further physiological investigations are warranted to determine whether these projections mediate the inhibition of the paralemniscal pathway by the lemniscal pathway.

3.3 Barrel field of the primary somatosensory cortex

The conventional understanding of whisker information processing depicts a bottom-up integration followed by a top-down propagation of neural activity, ultimately leading to the activation of facial muscles. However, our study reveals a more nuanced picture, demonstrating a bidirectional flow of information, with top-down regulation of sensory information from Bfd to the brainstem and thalamus through both excitatory and inhibitory monosynaptic connections.

Bfd extends long-range connections to lower-level structures within the whisker system. The barrel field excites PSV, the three thalamic nuclei we investigated (MOp, SC, and ZI), and inhibits PO, VPM, RT, MOp, SC, and ZI. Additionally, an uncategorized connection targeting SI was identified.

Transgenic and wild-type experiments revealed novel direct connections to SPVo, VII, and PPN. Our study also demonstrated top-down excitation of the trigeminal nucleus and facial motor nucleus by Bfd.

3.4 Primary Motor cortex

Primary motor cortex extensively targets nuclei across the cerebellar cortex and subcortical regions (see e.g.(**Bisman et al., 2011**, **Minju Jeong et al., 2016**, **Rodrigo Muñoz-Castañeda et al., 2021**). Our results show that there are parallel (i.e. excitatory and inhibitory) pathways of projections originating from the primary motor cortex and target bfd, PO, PPN, VTA, SC, VPM, RT, and ZI from MOp. Monosynaptic projections into these target nuclei have been described before (**Bisman et al., 2011**, **Minju Jeong et al., 2016**, **Rodrigo Muñoz-Castañeda et al., 2021**), except for a connection toward SPVc, that has been validated by at least two animal-lines. In addition to the aforementioned projections, uncategorized connections were found to target VII and the trigeminal nuclei. The observations on the parallel feed-forward excitatory and feed-forward inhibitory projections argue that the role of the motor cortical projections might have differential contribution to neural processing along ascending and descending pathways.

3.5 Superior Colliculus

In the map previously described by **Bosman et al., 2011**, the superior colliculus contribution to sensorimotor integration in the 18 nuclei map was limited to connections to ZI, PPN, and VII. Our study, however, revealed that SC was one of the most connected nodes in this network. Additionally, SC appears to be mainly the origin of inhibitory connections spanning across the entire sensorimotor and neuromodulatory systems. More specifically, inhibitory projections monosynaptically target MOp, ZI, the thalamus, bfd, VTA, SI, VPM, VII, PPN, and DR. The newly reported connections toward MOp and RT were validated in at least 2 different animal lines.

3.6 Facial motor nucleus

The facial motor nucleus, a key component of the descending motor pathway, is composed of motoneurons and sends commands to the periphery to produce whisker movement (**Ashwell, 1982**).

In this study, we found connections originating from VII targeting the trigeminal nuclei and SC. These structures, being the first nuclei to integrate whisker information in the brain, are also targeting VII (see the section \ref{trignuc}). The interplay between VII and the trigeminal nuclei might be

part of a low-level loop integrating sensory information and producing whisker movement without requiring activity from higher structures.

We also found that the facial motor nucleus excites PSV and SPVc. Connections that could not be definitively classified as excitatory or inhibitory (i.e. uncategorized) were found to target SPVo and SPVi. All of these connections were validated in at least 2 animal lines.

Reciprocal connections between the trigeminal nuclei and VII should be further investigated to understand the role of such low-level loops in the whisker system of the rodent. As VII does not send any inhibitory connections, based on the currently available data, one can assume the purely excitatory nature of the projections to SC. The postsynaptic target of facial motor nucleus projections into SC is not clear. If this connection targets the sensory area of SC, this suggests the possibility of an efference copy, a signal sent to SC to inform it about the action taken by the whisker and therefore, to adjust its internal representation based on previous movement.

3.7 Zona Incerta

The zona incerta is described as one of the main inhibition sources in the rodent whisker system (**Venkataraman et al., 2021**). Our study revealed that ZI could also send excitatory monosynaptic projections to every nucleus analyzed in our study, except for LC and TM. In addition, inhibitory connections were found to target MOp, the thalamic nuclei, VTA, SI, SC, PPN, and DR. New connections targeting bfd, PSV, SI, SPVo, VPM, VII, SPVc, SPVi and RT were identified in at least 2 animal lines. While most studies targeting ZI report GABAergic connections (**Ficalora and Mize, 1989**, **Nicolelis et al., 1992**, **Nicolelis et al., 1990**), the existence of the excitatory projections that target the entire sensorimotor network described herein suggest that ZI, along with SC, serves as a primary node of divergence in this network.

3.8 Neuromodulatory projections

The VTA has a role in learning the association of a whisker stimulus with a potential reward (**Esmaeili et al., 2020**). Our results revealed that the VTA's contribution to the whisker system's function is not necessarily solely mediated by dopaminergic connections; excitatory and inhibitory presynaptic neurons in the VTA also target other nuclei. The VTA sends excitatory connections to MOp, ZI, bfd, SI, RT, and DR and inhibitory projections to MOp, ZI, PO, bfd, SI, SC, TM, RT, and DR. Each of the new connections reported herein towards PO, bfd, PSV, SPVo, TM, VPM, PPN, SPVc and SPVi was confirmed at least in 2 animals lines.

Cholinergic connections have been hypothesized to play a role in transforming whisker sensations into a motor action (e.g. licking behavior (**Esmaeili et al., 2020**)). Consequently, it is not surprising to see connections originating from SI that target bfd and MOp. However, as for VTA, we observed a large

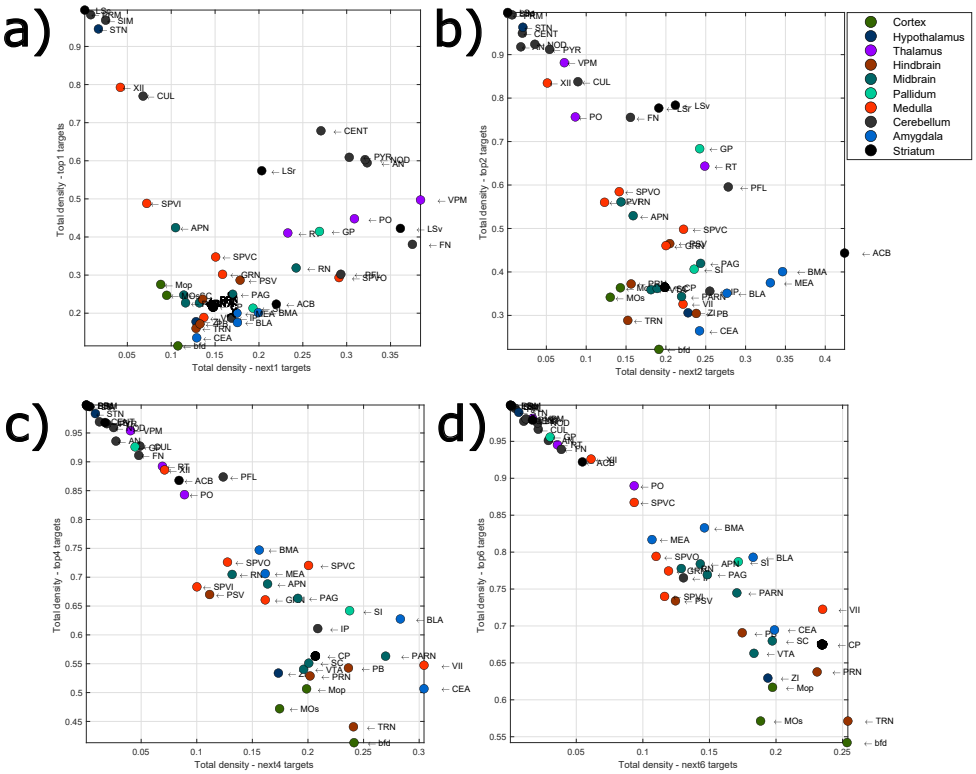

Fig. 6 Relative density of incoming connections. Connections were ordered by the density of incoming connections and plotted against the x next densest connections for comparison. This shows the skewness of the distribution. The color scale represents the anatomical structure to which the nuclei belong. **a)** The density of incoming connections as a function of the density of the next incoming connection (in order of magnitude) **b)** Same as a), but now for the next 2 connections. **c)** Same as a), but now for the next 4 connections. d) Same as a), but now for the next 6 connections.

number of connections, mainly inhibitory, targeting the other neuromodulator-releasing nuclei. This shows that SI can regulate the activity of other nuclei in the neuromodulatory system. In particular, SI inhibits PPN, another cholinergic nucleus. SI sends excitatory connections to MOp, ZI, bfd, and VTA, and inhibitory connections to MOp, ZI, bfd, VTA, SC, TM, PPN, RT, and DR. One connection with non-specific presynaptic cells was unveiled toward VII. New connections to SC, TM, and PPN were found in at least 2 animal lines.

Excitatory connections from DR were found to target MOp, ZI, bfd, VTA, SI, SC, PPN, and RT. The connections targeting ZI, PO, SI, and RT were validated by at least 2 animal lines.

3.9 Density distribution

To elucidate connectivity patterns within and between structures in the sensorimotor pathway, we conducted an analysis of the density, defined as the

percentage of outgoing connections originating from a single source, for each of the 57 nuclei (**Supplemental Figures 5 and 6**). This examination revealed distinctive connectivity profiles, with the cortex displaying sparse outgoing connections from a multitude of nuclei. The top 6 connections accounted for at most 62% of the outgoing density (**Figure 6.d**), emphasizing the distributed nature of cortical inputs. Contrastingly, structures such as the Cerebellum, Hypothalamus, and Striatum exhibited a more specialized pattern, with the top 4 of their outgoing projections accounting for over 85% of all of their projections (**Figure 6.c**).

When focusing on the ascending somatosensory pathway, a discernible pattern emerges. The trigeminal nuclei, serving as the initial nodes for whisker information, project sparsely to a diverse array of nuclei. Their top 6 projections targets explain approximately 80% of the outgoing projections (**Figure 6.d**). Subsequently, the pathway narrows as it targets the thalamus, projecting to fewer post-synaptic nuclei, with 75% of their outgoing density explained by only 2 projections (**Figure 6.a**). Finally, the cortical information flow displays a divergent pattern, with only 55% outgoing density distributed among 6 nuclei (**Figure 6.d**).

This observed pattern along the ascending somatosensory pathway underscores a dynamic process: the brainstem initially projects broadly, supporting a divergent network formation, followed by a sharp reduction of the target nuclei of the thalamus. The pathway then broadens again as cortical projections target a diverse set of nodes. This highlights the thalamus's specific role as a crucial node for routing sensory information. Coupled with inhibitory processes, the thalamus emerges as a key filter, emphasizing its pivotal role in shaping and modulating sensory inputs

3.10 Network analysis

To assess the role of neuromodulator-releasing nuclei in shaping the network structure and to investigate their potential facilitation of communication within the network, we conducted a permutation test with 10,000 permutations on the 57-nuclei adjacency matrix (**Supplemental Figure 4**). Comparisons between the network with and without neuromodulator-releasing nuclei revealed no discernible differences in terms of the distribution of betweenness centrality, degree centrality, nodal clustering, nodal efficiency, or local nodal efficiency. However, a notable distinction emerged in the comparison of nodal shortest path lengths. Specifically, the network without neuromodulator-releasing nuclei exhibited a significantly higher mean value (0.7766 \textpm 0.0812 std) compared to the network with neuromodulators (0.7564 \textpm 0.0964 std; p-value = \SI{7.99e-4}). These findings underscore the nuanced impact of neuromodulator-releasing nuclei on the structural dynamics of the network, particularly in terms of nodal shortest path lengths.

To determine if the network presented small-world properties, we compared the clustering coefficient and the shortest path between a structured graph (ER) and the 57x57 network resulting from our analysis of the Allen Brain

Database. This analysis revealed a significantly higher average shortest path for our network (mean ER = 0.6903 ±0.054 std; mean summary graph = 0.7564 ±0.0964 std; p-value = 9.999×10^{-5}) and a significantly higher clustering coefficient for our network (mean ER = 0.1537 ±0.0163 std; mean summary graph = 0.2377 ±0.1033 std; p-value = 9.999×10^{-5}). Given that our network presents a higher shortest path than an Erdos-Renyi graph (see Materials and Methods), we conclude that the studied network doesn't present a small-world structure.

Next, we computed the divergence ratio of each nucleus of the network (see section 2.4). This analysis revealed that the majority of the nuclei could not be clearly defined as convergent or divergent. Instead they exhibited a structurally balanced network with a balanced number of input and output connections. Outliers include the LC, which is a divergent node receiving inputs only from the Parabrachial Nucleus and sending connections to 8 nuclei. On the side of the spectrum, PO, PSV. SPVO, TM, VPM, VII, RT, FN, CUL, AN, NOD, CENT, SIM, PYR, COPY, PRM, STN, LA, PA, OT, and LSc appear as convergent nodes (**Figure 7**).

4 Discussion

We extended the established connectome of the mouse whisker system (**Bosman et al., 2011**) by incorporating 54 additional connections (**Figure 5**). This expansion involved a comprehensive analysis of a network comprising 57 nodes (**Supplementary Material - Fig.4**). Our focus centered on investigating connections within a subset of 18 nuclei, as outlined in the Introduction. Importantly, we substantiated the presence of these connections through anatomical evidence (**Supplementary Material - Fig.8 to Fig.21**). Within this framework, we identified cell-type-specific connections and calculated the divergence ratio of the examined nuclei. This analysis revealed intricate connectivity patterns along the ascending somatosensory pathway

We successfully identified a total of 138 connections, constituting 42.6% of all possible connections within this 18x18 subnetwork. Notably, 54 of these connections were not previously described in the literature, to the best of our knowledge. Given that the selection of the 18 nuclei was based on their experimentally confirmed contributions to sensorimotor integration, the observed high degree of connectivity appears plausible.

To ensure the robustness of our findings and mitigate potential biases from false positives or negatives, we conducted the analysis across different transgenic lines of animals (**Figure 4**). The connections included in our summary map (**Figure 5**) are exclusively those confirmed by at least two distinct animal lines

While the structures under consideration play a role in sensorimotor integration, it is plausible that some of the identified connections may not directly contribute to sensorimotor processing. Notably, certain structures (**Supplementary Material - Table 2**), such as neuromodulator-releasing

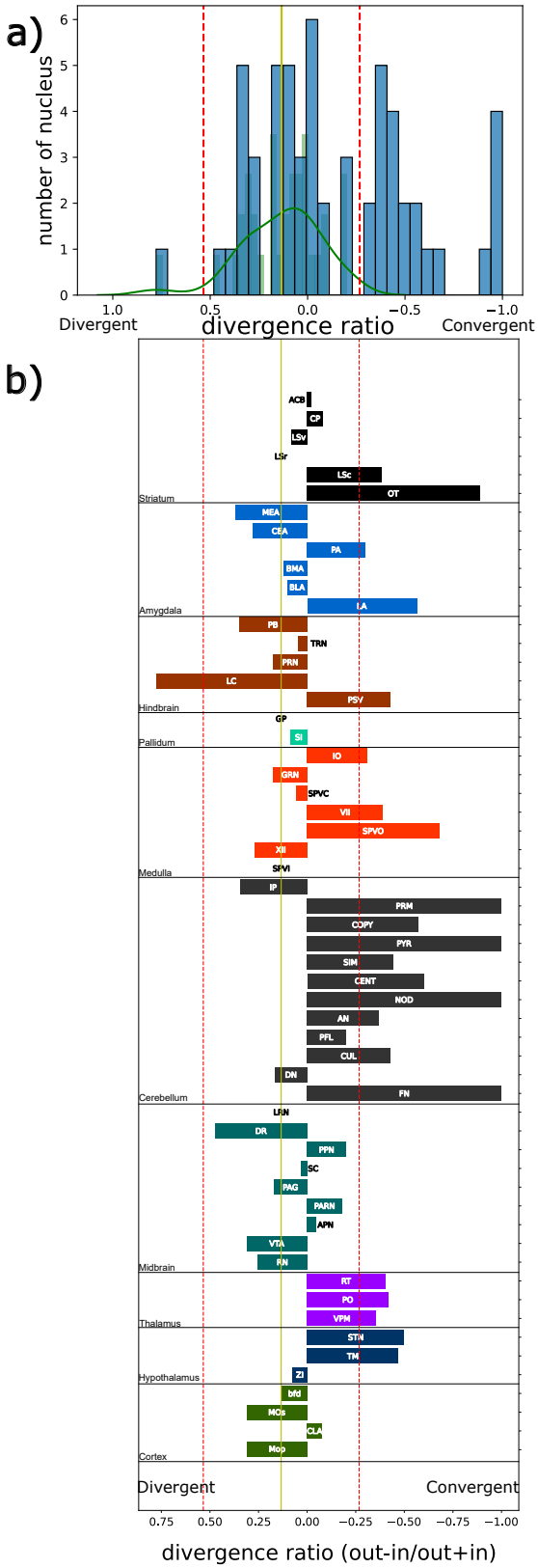
a)
number of nucleus
0
1
2
3
4
5
6
1.0
0.5
0.0
−0.5
−1.0
Divergent
divergence ratio
Convergent
b)
ACB
CP
LSv
LSr
LSc
OT
Striatum
MEA
CEA
PA
BMA
BLA
LA
Amygdala
PB
TRN
PRN
LC
PSV
Hindbrain
GP
SI
Pallidum
IO
GRN
SPVC
VII
SPVO
XII
SPVI
Medulla
IP
PRM
COPY
PYR
SIM
CENT
NOD
AN
PFL
CUL
DN
FN
Cerebellum
LRN
DR
PPN
SC
PAG
PARN
APN
VTA
RN
Midbrain
RT
PO
VPM
Thalamus
STN
TM
Hypothalamus
ZI
bfd
MOs
CLA
Mop
Cortex
Divergent
Convergent
0.75
0.50
0.25
0.00
−0.25
−0.50
−0.75
−1.00
divergence ratio (out-in/out+in)

Fig. 7 Divergence ratio of the nuclei a) Divergence ratio distribution and **b)** Divergence ratio of the 57-nodes network. The yellow line represents the mean of the distribution centered around the population of balanced nodes (see Material and Methods), and the red dotted lines represent the mean ± two times the standard deviation.

nuclei, were targeted by only a few, if any, experiments. These connections warrant further investigation to better understand their functional significance.

Despite the absence of small-world properties in our network analysis results, it is crucial to consider that we preselected a highly interconnected network wherein every nucleus plays a distinct role. These findings suggest that even if some nuclei were 'cut' from the network, information flow could persist, underscoring the robustness of the network organization. Conversely, the analysis of shortest-path length highlights the importance of neuromodulator-releasing nuclei in facilitating faster communication between network nodes. The average shortest path length significantly increases in the absence of these nuclei.

Inhibition is a pervasive phenomenon at every level in the whisker system. Our study reveals inhibitory contributions from nodes not previously identified as sources of inhibition. A notable example is the inhibitory connection from VPM to PO, as illustrated in the Ppp1r17-Cre-NL1 animal line (**Supplementary Material - Fig7**). This discovery challenges the notion that RT is the sole source of inhibition in the somatosensory thalamus. The inhibitory pathway from VPM may even play a role in disinhibition, given its targeting of RT and ZI, which, in turn, influence the thalamic nuclei of the ascending somatosensory pathway (**Figure 4**). This suggests a nuanced filtering or processing role for VPM beyond its traditional role as a relay station.

Inhibition is not confined to higher levels; it is also observed in the trigeminal nuclei, which send inhibitory connections (**Figure 4**). While these connections primarily target other trigeminal nuclei, especially VII, they may play a crucial role in modulating whisker movement amplitude following contact with an object during free whisking. Descending projecting connections from higher-level structures could then further modulate whisking behavior during active exploration. This low-level loop in the whisker system underscores the ability of trigeminal nuclei to reduce whisking amplitude upon contact with an object. Furthermore, ascending inhibitory connections from the somatosensory brainstem (trigeminal nuclei) target VPM and PPN, suggesting a multifaceted role for the trigeminal nuclei beyond a simple relay station in the whisker system. In conclusion, our analysis points to extensive and intricate processing that involves both excitatory and inhibitory projections in the early phases of the somatosensory pathway, as it was previously described in invertebrates for sensorimotor control (**Hugues and Celikel, 2019**)

The connectivity pattern of the ascending somatosensory pathway follows an hourglass shape, with a divergent brainstem projections, followed by convergence of thalamus projections into only a few targets in the cortex. Once

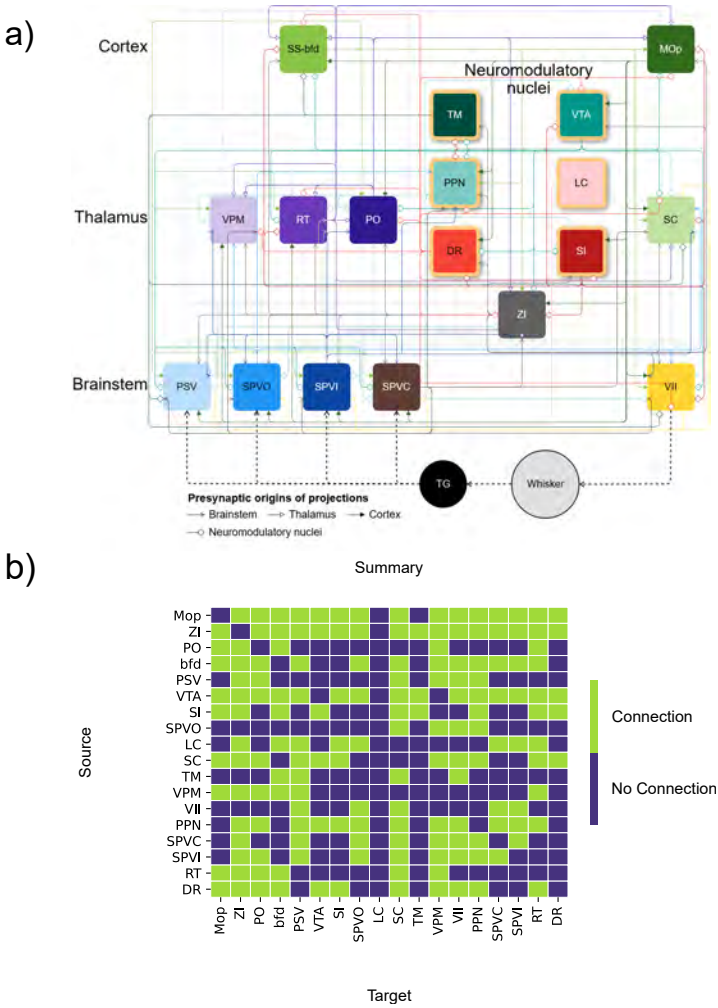

Fig. 8 The sensorimotor connectivity map of the mouse whisker system. Summary of data from all animal lines combined. **a)** A total of 180 connections were found and confirmed either by previous work or by at least two different types of mice. The dashed lines represent the flow of information outside of the central nervous system. The neuromodulatory structures are represented with yellow borders. **b)** A binary connectivity matrix that summarizes the pairwise connectivity in the network.

the sensory information reaches the cortex, the divergence of projections once again allows the distribution of the sensory information across large number of nuclei. This is further supported by the results shown from our analysis of outgoing densities (**Figure 6**). In fact, this analysis demonstrates that the trigeminal nuclei are nodes that distribute information beyond sensory thalamus. Meanwhile, the narrowing of the pathway at the level of the thalamus through denser and fewer connections, together with the presence of inhibition in this structure, might hint at a filtering role of the somatosensory thalamus,

as it appears to be highly specialized given the few strong connections originating from this structure (**Figure 7**). Further widening of the projections in the cortex points to a possible parallel processing of sensory information along the downstream nuclei.

Top-down regulation is a prominent feature in the somatosensory system, occurring both between the barrel field cortex (bfd) and the thalamus and between the thalamus and the trigeminal nuclei. Inhibition, particularly originating in bfd and targeting VPM, RT, and PO, complements excitatory connections, allowing for effective top-down modulation of somatosensory thalamic activity. Additionally, a direct top-down connection from VPM to PSV highlights the regulatory influence in the lemniscal pathway.

The Ventral Tegmental Area (VTA) stands out for targeting 15 out of 17 nuclei in our subnetwork, with intriguingly no incoming connections from the somatosensory system. Instead, the VTA primarily receives input from other neuromodulator-releasing nuclei, along with inputs from ZI and MOp. This arrangement suggests that MOp may modulate activity in nodes of the ascending somatosensory pathway through the VTA. The VTA is the only neuromodulator-releasing nucleus with such a wide variety of targets. LC seems to target mainly structures of the sensory system. SI doesn't appear to have a role in the regulation of activity in low-level structures, as no connections toward the trigeminal nuclei nor VII could be confirmed. PPN situates itself on the opposite end of the spectrum, as not a single structure from the cortex appears to be targeted. Notably, the neuromodulator-releasing nuclei display a high degree of interconnectedness, allowing for mutual modulation.

Leveraging the Allen Brain database, we identified 54 new connections, categorizing their nature and enhancing our understanding of the subnetwork's connectome. Our analysis emphasizes the role of both low-level structures and neuromodulator-releasing nuclei, revealing the widespread occurrence of inhibition at various stages of information processing. While this study provides a clearer picture of how the sensorimotor pathway integrates whisker information, further investigations, including functional studies and testing with additional transgenic lines, are necessary to elucidate the specific roles of each connection in sensorimotor integration. The road to a comprehensive understanding of the rodent whisker system's sensorimotor pathway requires more extensive tracing experiments, particularly with higher granularity on low-level structures and neuromodulator-releasing nuclei, to pave the way for the development of a biologically inspired computational model of the entire network

Are mice small rats?

In their prior study, Bosman et al. (**2011**) considered connections from various rodent species, encompassing both rats and mice, assuming uniformity across the whisker systems of different rodent subspecies. However, a review by Krubitzer et al. (**Krubitzer et al., 2011**) highlighted significant anatomical differences in rodents, particularly between rats and mice. Despite these

differences, the two species are often treated interchangeably in anatomical structure sizes or positions, raising questions about the relevance of employing an average model for the broader category of rodents, where connections are constrained by brain anatomy.

The connections we demonstrate in this study are based on experiments conducted specifically on mice, avoiding the potential constraint imposed by assuming a uniform rodent model. Nevertheless, the original connections we build upon were not observed in studies that differentiated between rats and mice. To thoroughly assess the similarity between the rat and mouse connectome, further translational anatomical studies will be necessary.

Shortcomings of the experimental approach

We used anatomical data collected through serial 2-photon tomography, made available by the Allen Brain Institute, to confirm targets and the source of monosynaptic connection. This method allows visualization of the expressions of genetically encoded fluorescent proteins in anatomically targeted regions using cell-type-specific or non-specific promoters in various animal lines. However, it's important to note that the spatial resolution of this technique is not sufficient to resolve individual synapses, thus it is not always possible to reliably distinguish en-passant projections from actual terminals. Additionally, the sensorimotor circuit outlined in our analysis is derived from anterograde tracing experiments. To further refine our understanding, trans-synaptic tracing of each discussed connection would be beneficial, enabling differentiation between en-passant fibers and terminals and providing cell-type information for the pre- and post-synaptic neurons.

Our results are based on the analysis of data from 732 different experiments. To anatomically confirm the presence of the connections mentioned in our results section and depicted in our summary map (**Figure 8**), we employed two-photon tomography imaging in brain slices. However, challenges arose during the alignment of the normalized brain atlas to each image due to variations in cut angles. Furthermore, tissue alterations caused by cuts, such as squishing, and potential tissue shrinkage induced by the fixation solution injection added complexity to the alignment process. The inherent discretization of imaging data, in contrast to the continuous nature of data analysis, also presented challenges in achieving accurate alignment between the normalized brain and imaging data.

Conclusions

Leveraging the Allen Brain database, we identified 54 new connections, categorizing their nature and enhancing our understanding of the subnetwork's connectome. Our analysis emphasizes the role of both low-level structures and neuromodulator-releasing nuclei, revealing the widespread occurrence of inhibition at various stages of information processing. While this study provides

a clearer picture of how the sensorimotor pathway integrates whisker information as well as the contributions of the top-down and neuromodulatory circuits, further investigations, including functional studies and testing with additional transgenic lines, are necessary to elucidate the specific roles of each connection in sensorimotor integration. The road to a comprehensive understanding of the rodent whisker system's sensorimotor pathway requires more extensive circuit analysis, including trans-synaptic tracing experiments, particularly with higher granularity on low-level structures and neuromodulator-releasing nuclei, to pave the way for the development of a biologically inspired computational model of the entire network.

Acknowledgment

This project has received funding from the European Union's Horizon 2020 research and innovation program under the Marie Skłodowska-Curie grant agreement No 860949.

References

[1] Ahissar, E., & Arieli, A. (2001). Figuring Space by Time. Neuron, 32(2), 185–201. https://doi.org/10.1016/s0896-6273(01)00466-4

[2] An, S., Li, X., Deng, L., Zhao, P., Ding, Z., Han, Y., ... & Gong, H. (2021). A whole-brain connectivity map of VTA and SNc glutamatergic and GABAergic neurons in mice. Frontiers in Neuroanatomy, 15, 818242.

[3] Aransay, A. M., Rodríguez-López, C., García-Amado, M. A., Clascá, F., & Prensa, L. (2015). Long-range projection neurons of the mouse ventral tegmental area: a single-cell axon tracing analysis. Frontiers in Neuroanatomy, 9. https://doi.org/10.3389/fnana.2015.00059

[4] Ashwell KW. The adult mouse facial nerve nucleus: morphology and musculotopic organization. J Anat. 1982 Oct;135(Pt 3):531-8. PMID: 7153172; PMCID: PMC1169402.

[5] Azarfar, A., Calcini, N., Huang, C., Zeldenrust, F., & Celikel, T. (2018). Neural coding: A single neuron's perspective. Neuroscience & Biobehavioral Reviews, 94, 238-247.

[6] Bartho, P., Freund, T. F., & Acsády, L. (2002). Selective GABAergic innervation of thalamic nuclei from zona incerta. European Journal of Neuroscience, 16(6), 999-1014.

[7] Bellavance, M. A., Takatoh, J., Lu, J., Demers, M., Kleinfeld, D., Wang, F., & Deschênes, M. (2017). Parallel inhibitory and excitatory trigemino-facial feedback circuitry for reflexive vibrissa movement. Neuron, 95(3), 673-682.

[8] Benavidez, N. L., Bienkowski, M. S., Zhu, M., Garcia, L. H., Fayzullina, M., Gao, L., ... & Dong, H. W. (2021). Organization of the inputs and outputs of the mouse superior colliculus. Nature communications, 12(1), 4004.

[9] Bosman, L. W. J., Houweling, A. R., Owens, C. B., Tanke, N., Shevchouk, O. T., Rahmati, N., Teunissen, W. H. T., Ju, C., Gong, W., Koekkoek, S. K. E., & de Zeeuw, C. I. (2011). Anatomical Pathways Involved in Generating and Sensing Rhythmic Whisker Movements. Frontiers in Integrative Neuroscience, 5. https://doi.org/10.3389/fnint.2011.00053

[10] Cheng L, Arata A, Mizuguchi R, Qian Y, Karunaratne A, Gray PA, Arata S, Shirasawa S, Bouchard M, Luo P, Chen CL, Busslinger M, Goulding M, Onimaru H, Ma Q. Tlx3 and Tlx1 are post-mitotic selector genes determining glutamatergic over GABAergic cell fates. Nat Neurosci. 2004 May;7(5):510-7. doi: 10.1038/nn1221. Epub 2004 Apr 4. PMID: 15064766.

[11] Chiaia, N.L., Rhoades, R.W., Bennett-Clarke, C.A., Fish, S.E. and Killackey, H.P. (1991), Thalamic processing of vibrissal information in the rat. I. Afferent input to the medial ventral posterior and posterior nuclei. J. Comp. Neurol., 314: 201-216. https://doi.org/10.1002/cne.903140202

[12] Daigle TL, Madisen L, Hage TA, Valley MT, Knoblich U, Larsen RS, Takeno MM, Huang L, Gu H, Larsen R, Mills M, Bosma-Moody A, Siverts LA, Walker M, Graybuck LT, Yao Z, Fong O, Nguyen TN, Garren E, Lenz GH, Chavarha M, Pendergraft J, Harrington J, Hirokawa KE, Harris JA, Nicovich PR, McGraw MJ, Ollerenshaw DR, Smith KA, Baker CA, Ting JT, Sunkin SM, Lecoq J, Lin MZ, Boyden ES, Murphy GJ, da Costa NM, Waters J, Li L, Tasic B, Zeng H. A Suite of Transgenic Driver and Reporter Mouse Lines with Enhanced Brain-Cell-Type Targeting and Functionality. Cell. 2018 Jul 12;174(2):465-480.e22. doi: 10.1016/j.cell.2018.06.035. PMID: 30007418; PMCID: PMC6086366.

[13] Daigle, T. L., Madisen, L., Hage, T. A., Valley, M. T., Knoblich, U., Larsen, R. S., ... & Zeng, H. (2018). A suite of transgenic driver and reporter mouse lines with enhanced brain-cell-type targeting and functionality. Cell, 174(2), 465-480.

[14] Dorocic, I. P., Fürth, D., Xuan, Y., Johansson, Y., Pozzi, L., Silberberg, G., ... & Meletis, K. (2014). A whole-brain atlas of inputs to serotonergic neurons of the dorsal and median raphe nuclei. Neuron, 83(3), 663-678.

[15] Dunigan, A. I., Swanson, A. G., Olson, D. L., & Roseberry, A. G. (2021). Whole-brain efferent and afferent connectivity of mouse ventral tegmental area melanocortin-3 receptor neurons. Journal of Comparative Neurology, 529(6), 1157–1183. https://doi.org/10.1002/cne.25013

[16] Esmaeili, V., Tamura, K., Foustoukos, G., Oryshchuk, A., Crochet, S., & Petersen, C. C. (2020). Cortical circuits for transforming whisker sensation into goal-directed licking. Current Opinion in Neurobiology, 65, 38-48.

[17] Ficalora, A. S., & Mize, R. R. (1989). The neurons of the substantia nigra

and zona incerta which project to the cat superior colliculus are GABA immunoreactive: a double-label study using GABA immunocytochemistry and lectin retrograde transport. Neuroscience, 29(3), 567-581.

[18] Furuta, T., Timofeeva, E., Nakamura, K., Okamoto-Furuta, K., Togo, M., Kaneko, T., & Deschenes, M. (2008). Inhibitory Gating of Vibrissal Inputs in the Brainstem. Journal of Neuroscience, 28(8), 1789–1797. https://doi.org/10.1523/jneurosci.4627-07.2008

[19] Harris JA, Hirokawa KE, Sorensen SA, Gu H, Mills M, Ng LL, Bohn P, Mortrud M, Ouellette B, Kidney J, Smith KA, Dang C, Sunkin S, Bernard A, Oh SW, Madisen L, Zeng H. Anatomical characterization of Cre driver mice for neural circuit mapping and manipulation. Front Neural Circuits. 2014 Jul 10;8:76. doi: 10.3389/fncir.2014.00076. PMID: 25071457; PMCID: PMC4091307.

[20] Hattox, A., Li, Y., & Keller, A. (2003). Serotonin Regulates Rhythmic Whisking. Neuron, 39(2), 343–352. https://doi.org/10.1016/s0896-6273(03)00391-x

[21] Hayashi, H. (1980). Distributions of vibrissae afferent fiber collaterals in the trigeminal nuclei as revealed by intra-axonal injection of horseradish peroxidase. *Brain Research*, *183*(2), 442–446. https://doi.org/10.1016/0006-8993(80)90478-3

[22] Hemelt, M. E., & Keller, A. (2008). Superior Colliculus Control of Vibrissa Movements. Journal of Neurophysiology, 100(3), 1245–1254. https://doi.org/10.1152/jn.90478.2008

[23] Hooks, B. M., Mao, T., Gutnisky, D. A., Yamawaki, N., Svoboda, K., & Shepherd, G. M. (2013). Organization of cortical and thalamic input to pyramidal neurons in mouse motor cortex. Journal of Neuroscience, 33(2), 748-760.

[24] Hosp, J. A., Pekanovic, A., Rioult-Pedotti, M. S., & Luft, A. R. (2011). Dopaminergic Projections from Midbrain to Primary Motor Cortex Mediate Motor Skill Learning. The Journal of Neuroscience, 31(7), 2481–2487. https://doi.org/10.1523/jneurosci.5411-10.2011

[25] Hughes, S., & Celikel, T. (2019). Prominent Inhibitory Projections Guide Sensorimotor Computation: an invertebrate perspective. *BioEssays*, *41*(10). https://doi.org/10.1002/bies.201900088

[26] Isa, T., Marquez-Legorreta, E., Grillner, S., & Scott, E. K. (2021). The tectum/superior colliculus as the vertebrate solution for spatial sensory integration and action. Current Biology, 31(11), R741–R762. https://doi.org/10.1016/j.cub.2021.04.001

[27] Jacquin, M. F., Chiaia, N. L., Haring, J. H., & Rhoades, R. W. (1990). Intersubnuclear connections within the rat trigeminal brainstem complex. Somatosensory & motor research, 7(4), 399-420.

[28] Jeong, M., Kim, Y., Kim, J., Ferrante, D. D., Mitra, P. P., Osten, P., & Kim, D. (2016). Comparative three-dimensional connectome map of motor cortical projections in the mouse brain. Scientific reports, 6(1), 1-14.

[29] Kleinfield, D., W. Berg, R. & M. Connor, S. (1999) Invited Review

Anatomical loops and their electrical dynamics in relation to whisking by rat, Somatosensory & Motor Research, 16(2), 69-88, DOI: 10.1080/08990229970528

[30] Krubitzer, L., Campi, K. L., & Cooke, D. F. (2011). All rodents are not the same: a modern synthesis of cortical organization. *Brain Behavior and Evolution*, *78*(1), 51–93. https://doi.org/10.1159/000327320

[31] Lam, Y. W., & Sherman, S. M. (2007). Different topography of the reticulothalmic inputs to first-and higher-order somatosensory thalamic relays revealed using photostimulation. Journal of neurophysiology, 98(5), 2903-2909.

[32] Leão RN, Mikulovic S, Leão KE, Munguba H, Gezelius H, Enjin A, Patra K, Eriksson A, Loew LM, Tort AB, Kullander K. OLM interneurons differentially modulate CA3 and entorhinal inputs to hippocampal CA1 neurons. Nat Neurosci. 2012 Nov;15(11):1524-30. doi: 10.1038/nn.3235. Epub 2012 Oct 7. PMID: 23042082; PMCID: PMC3483451.

[33] Lee, S., Carvell, G. E., & Simons, D. J. (2008). Motor modulation of afferent somatosensory circuits. Nature Neuroscience, 11(12), 1430–1438. https://doi.org/10.1038/nn.2227

[34] Lee, S. H., & Dan, Y. (2012). Neuromodulation of Brain States. Neuron, 76(1), 209–222. https://doi.org/10.1016/j.neuron.2012.09.012

[35] Liu, X., Huang, H., Snutch, T.P. et al. The Superior Colliculus: Cell Types, Connectivity, and Behavior. Neurosci. Bull. 38, 1519–1540 (2022). https://doi.org/10.1007/s12264-022-00858-1

[36] Ma, P. M. (1991). The barrelettes—architectonic vibrissal representations in the brainstem trigeminal complex of the mouse. Normal structural organization. Journal of Comparative Neurology, 309(2), 161-199.

[37] Madisen L, Zwingman TA, Sunkin SM, Oh SW, Zariwala HA, Gu H, Ng LL, Palmiter RD, Hawrylycz MJ, Jones AR, Lein ES, Zeng H. A robust and high-throughput Cre reporting and characterization system for the whole mouse brain. Nat Neurosci. 2010 Jan;13(1):133-40. doi: 10.1038/nn.2467. Epub 2009 Dec 20. PMID: 20023653; PMCID: PMC2840225.

[38] McElvain, L. E., Friedman, B., Karten, H. J., Svoboda, K., Wang, F., Deschênes, M., & Kleinfeld, D. (2018). Circuits in the Rodent Brainstem that Control Whisking in Concert with Other Orofacial Motor Actions. Neuroscience, 368, 152–170. https://doi.org/10.1016/j.neuroscience.2017.08.034

[39] Morrow JA, Collie IT, Dunbar DR, Walker GB, Shahid M, Hill DR. Molecular cloning and functional expression of the human glycine transporter GlyT2 and chromosomal localisation of the gene in the human genome. FEBS Lett. 1998 Nov 20;439(3):334-40. doi: 10.1016/s0014-5793(98)01390-8. PMID: 9845349.

[40] Muñoz-Castañeda, R., Zingg, B., Matho, K.S. et al. Cellular anatomy of the mouse primary motor cortex. Nature 598, 159–166 (2021). https://doi.org/10.1038/s41586-021-03970-w

[41] Nicolelis, M. A., Chapin, J. K., & Lin, R. C. (1992). Somatotopic maps

within the zona incerta relay parallel GABAergic somatosensory pathways to the neocortex, superior colliculus, and brainstem. Brain research, 577(1), 134-141.

[42] Nicolelis, M., & Chapin, J. (1994). Spatiotemporal structure of somatosensory responses of many-neuron ensembles in the rat ventral posterior medial nucleus of the thalamus. The Journal of Neuroscience, 14(6), 3511–3532. https://doi.org/10.1523/jneurosci.14-06-03511.1994

[43] Oh, S. W., Harris, J. A., Ng, L., Winslow, B., Cain, N., Mihalas, S., ... & Zeng, H. (2014). A mesoscale connectome of the mouse brain. Nature, 508(7495), 207-214.

[44] Parolari, L. (2020). Dissection of Neurons and Circuits Involved in Regulating Innate Behaviors, Movement and Higher Cognitive Functions in Mice.

[45] Pinault, D., Bourassa, J., & Deschênes, M. (1995). The axonal arborization of single thalamic reticular neurons in the somatosensory thalamus of the rat. *European Journal of Neuroscience*, *7*(1), 31–40. https://doi.org/10.1111/j.1460-9568.1995.tb01017.x

[46] Plummer, N. W., Chandler, D. J., Powell, J. A., Scappini, E., Waterhouse, B. D., & Jensen, P. (2020). An intersectional Viral-Genetic method for fluorescent tracing of axon collaterals reveals details of noradrenergic locus coeruleus structure. ENeuro, 7(3), ENEURO.0010-20.2020. https://doi.org/10.1523/eneuro.0010-20.2020

[47] Rang, H. P., Dale, M. M., Ritter, J. M., Flower, R. J., & Henderson, G. (2015). Rang and Dale's Pharmacology.

[48] Ruhl DA, Bomba-Warczak E, Watson ET, Bradberry MM, Peterson TA, Basu T, Frelka A, Evans CS, Briguglio JS, Basta T, Stowell MHB, Savas JN, Roopra A, Pearce RA, Piper RC, Chapman ER. Synaptotagmin 17 controls neurite outgrowth and synaptic physiology via distinct cellular pathways. Nat Commun. 2019 Aug 6;10(1):3532. doi: 10.1038/s41467-019-11459-4. PMID: 31387992; PMCID: PMC6684635.

[49] Safran M, Dalah I, Alexander J, Rosen N, Iny Stein T, Shmoish M, Nativ N, Bahir I, Doniger T, Krug H, Sirota-Madi A, Olender T, Golan Y, Stelzer G, Harel A, Lancet D. GeneCards Version 3: the human gene integrator. Database (Oxford). 2010 Aug 5;2010:baq020. doi: 10.1093/database/baq020. PMID: 20689021; PMCID: PMC2938269.

[50] Lee, E. Y., Hwang, Y. G., & Lee, H. S. (2017). Hypothalamic neuronal origin of neuropeptide Y (NPY) or cocaine- and amphetamine-regulated transcript (CART) fibers projecting to the tuberomammillary nucleus of the rat. Brain Research, 1657, 16-28. https://doi.org/10.1016/j.brainres.2016.11.025

[51] Shao-Ming Lu & Rick C.-S. Lin (1993) Thalamic Afferents of the Rat Barrel Cortex: A Light-and Electron-Microscopic Study Using Phaseolus vulgaris Leucoagglutinin as an Anterograde Tracer, Somatosensory & Motor Research, 10:1, 1-16, DOI: 10.3109/08990229309028819

[52] Smith, J. B., Watson, G. D., Alloway, K. D., Schwarz, C., & Chakrabarti,

S. (2015). Corticofugal projection patterns of whisker sensorimotor cortex to the sensory trigeminal nuclei. Frontiers in Neural Circuits, 9, 160040. https://doi.org/10.3389/fncir.2015.00053

[53] Sokhadze, G., Campbell, P. W., & Guido, W. (2019). Postnatal development of cholinergic input to the thalamic reticular nucleus of the mouse. European Journal of Neuroscience, 49(8), 978-989.

[54] Stacey D, Bilbao A, Maroteaux M, Jia T, Easton AC, Longueville S, Nymberg C, Banaschewski T, Barker GJ, Büchel C, Carvalho F, Conrod PJ, Desrivières S, Fauth-Bühler M, Fernandez-Medarde A, Flor H, Gallinat J, Garavan H, Bokde AL, Heinz A, Ittermann B, Lathrop M, Lawrence C, Loth E, Lourdusamy A, Mann KF, Martinot JL, Nees F, Palkovits M, Paus T, Pausova Z, Rietschel M, Ruggeri B, Santos E, Smolka MN, Staehlin O, Jarvelin MR, Elliott P, Sommer WH, Mameli M, Müller CP, Spanagel R, Girault JA, Schumann G; IMAGEN Consortium. RASGRF2 regulates alcohol-induced reinforcement by influencing mesolimbic dopamine neuron activity and dopamine release. Proc Natl Acad Sci U S A. 2012 Dec 18;109(51):21128-33. doi: 10.1073/pnas.1211844110. Epub 2012 Dec 5. PMID: 23223532; PMCID: PMC3529066.

[55] Sumser, A., Mease, R. A., Sakmann, B., & Groh, A. (2017). Organization and somatotopy of corticothalamic projections from L5B in mouse barrel cortex. Proceedings of the National Academy of Sciences, 114(33), 8853-8858. https://doi.org/10.1073/pnas.1704302114

[56] Sun, P., Wang, J., Zhang, M., Duan, X., Wei, Y., Xu, F., ... & Zhang, Y. H. (2020). Sex-related differential whole-brain input atlas of locus coeruleus noradrenaline neurons. Frontiers in Neural Circuits, 14, 53.

[57] Takatoh, J., Park, J. H., Lu, J., Li, S., Thompson, P. M., Han, B. X., ... & Wang, F. (2021). Constructing an adult orofacial premotor atlas in Allen mouse CCF. Elife, 10.

[58] Taniguchi H, He M, Wu P, Kim S, Paik R, Sugino K, Kvitsiani D, Fu Y, Lu J, Lin Y, Miyoshi G, Shima Y, Fishell G, Nelson SB, Huang ZJ. A resource of Cre driver lines for genetic targeting of GABAergic neurons in cerebral cortex. Neuron. 2011 Sep 22;71(6):995-1013. doi: 10.1016/j.neuron.2011.07.026. Epub 2011 Sep 21. Erratum in: Neuron. 2011 Dec 22;72(6):1091. Kvitsani, Duda [corrected to Kvitsiani, Duda]. PMID: 21943598; PMCID: PMC3779648.

[59] Tasic B, Menon V, Nguyen TN, Kim TK, Jarsky T, Yao Z, Levi B, Gray LT, Sorensen SA, Dolbeare T, Bertagnolli D, Goldy J, Shapovalova N, Parry S, Lee C, Smith K, Bernard A, Madisen L, Sunkin SM, Hawrylycz M, Koch C, Zeng H. Adult mouse cortical cell taxonomy revealed by single cell transcriptomics. Nat Neurosci. 2016 Feb;19(2):335-46. doi: 10.1038/nn.4216. Epub 2016 Jan 4. PMID: 26727548; PMCID: PMC4985242.

[60] Tritsch NX, Oh WJ, Gu C, Sabatini BL. Midbrain dopamine neurons sustain inhibitory transmission using plasma membrane uptake of GABA, not synthesis. Elife. 2014 Apr 24;3:e01936. doi: 10.7554/eLife.01936. PMID:

24843012; PMCID: PMC4001323.

[61] Uhlén M, Fagerberg L, Hallström BM, Lindskog C, Oksvold P, Mardinoglu A, Sivertsson Å, Kampf C, Sjöstedt E, Asplund A, Olsson I, Edlund K, Lundberg E, Navani S, Szigyarto CA, Odeberg J, Djureinovic D, Takanen JO, Hober S, Alm T, Edqvist PH, Berling H, Tegel H, Mulder J, Rockberg J, Nilsson P, Schwenk JM, Hamsten M, von Feilitzen K, Forsberg M, Persson L, Johansson F, Zwahlen M, von Heijne G, Nielsen J, Pontén F. Proteomics. Tissue-based map of the human proteome. Science. 2015 Jan 23;347(6220):1260419. doi: 10.1126/science.1260419. PMID: 25613900.

[62] Urbain, N., & Deschênes, M. (2007). Motor cortex gates vibrissal responses in a thalamocortical projection pathway. *Neuron*, *56*(4), 714–725. https://doi.org/10.1016/j.neuron.2007.10.023

[63] Venkataraman, A., Hunter, S. C., Dhinojwala, M., Ghebrezadik, D., Guo, J., Inoue, K., Young, L. J., & Dias, B. G. (2021). Incerto-thalamic modulation of fear via GABA and dopamine. Neuropsychopharmacology, 46(9), 1658-1668. https://doi.org/10.1038/s41386-021-01006-5

[64] Voigts, J., Sakmann, B., & Celikel, T. (2008). Unsupervised Whisker Tracking in Unrestrained Behaving Animals. Journal of Neurophysiology, 100(1), 504–515. https://doi.org/10.1152/jn.00012.2008

[65] Voigts, J., Herman, D., & Celikel, T. (2015). Tactile object localization by anticipatory whisker motion. Journal of Neurophysiology, 113(2), 620–632. https://doi.org/10.1152/jn.00241.2014

[66] Volta M, Viaro R, Trapella C, Marti M, Morari M. Dopamine-nociceptin/orphanin FQ interactions in the substantia nigra reticulata of hemiparkinsonian rats: involvement of D2/D3 receptors and impact on nigro-thalamic neurons and motor activity. Exp Neurol. 2011 Mar;228(1):126-37. doi: 10.1016/j.expneurol.2010.12.024. Epub 2011 Jan 6. PMID: 21215744.

[67] Vitrac, C., & Benoît-Marand, M. (2017). Monoaminergic modulation of motor cortex function. Frontiers in Neural Circuits, 11. https://doi.org/10.3389/fncir.2017.00072

[68] Wang, J., Wang, X., Xia, M., Liao, X., Evans, A., & He, Y. (2015). GRETNA: a graph theoretical network analysis toolbox for imaging connectomics. Frontiers in human neuroscience, 9, 386.

[69] Wang, Q., Ding, S. L., Li, Y., Royall, J., Feng, D., Lesnar, P., Graddis, N., Naeemi, M., Facer, B., Ho, A., Dolbeare, T., Blanchard, B., Dee, N., Wakeman, W., Hirokawa, K. E., Szafer, A., Sunkin, S. M., Oh, S. W., Bernard, A., . . . Ng, L. (2020). The Allen Mouse Brain Common Coordinate Framework: A 3D Reference Atlas. Cell, 181(4), 936–953.e20. https://doi.org/10.1016/j.cell.2020.04.007

[70] Watts, D. J., & Strogatz, S. H. (1998). Collective dynamics of 'small-world'networks. nature, 393(6684), 440-442.

[71] Woolsey, T. A., & Van der Loos, H. (1970). The structural organization of layer IV in the somatosensory region (SI) of mouse cerebral cortex: the description of a cortical field composed of discrete cytoarchitectonic units.

Brain research, 17(2), 205-242.

[72] Yang, Y., Jiang, T., Jia, X., Yuan, J., Li, X., & Gong, H. (2022). Whole-Brain Connectome of GABAergic Neurons in the Mouse Zona Incerta. Neuroscience Bulletin, 1-15.

[73] Zakiewicz, I. M., Bjaalie, J. G., & Leergaard, T. B. (2014). Brain-wide map of efferent projections from rat barrel cortex. Frontiers in Neuroinformatics, 8. https://doi.org/10.3389/fninf.2014.00005

[74] Zeisel A, Hochgerner H, Lönnerberg P, Johnsson A, Memic F, van der Zwan J, Häring M, Braun E, Borm LE, La Manno G, Codeluppi S, Furlan A, Lee K, Skene N, Harris KD, Hjerling-Leffler J, Arenas E, Ernfors P, Marklund U, Linnarsson S. Molecular Architecture of the Mouse Nervous System. Cell. 2018 Aug 9;174(4):999-1014.e22. doi: 10.1016/j.cell.2018.06.021. PMID: 30096314; PMCID: PMC6086934.

[75] Zhou, M., Liu, Z., Melin, M.D. et al. A central amygdala to zona incerta projection is required for acquisition and remote recall of conditioned fear memory. Nat Neurosci 21, 1515–1519 (2018). https://doi.org/10.1038/s41593-018-0248-4

Supplementary Materials

TG line	Classification	Source
A930038C07Rik-Tg1-Cre	Excitatory	Harris et al., 2014
Adycap1-2A-Cre	Uncategorized	Zeisel et al., 2018
Calb2-IRES-Cre	Inhibitory	Taniguchi et al., 2011
Calb1-T2A-dgCre	Inhibitory	Daigle et al., 2018
Cart-IRES2-Cre	Uncategorized	Zeisel et al., 2018
Cart-Tg1-Cre	Uncategorized	Zeisel et al., 2018
Cck-IRES-Cre	Uncategorized	Taniguchi et al., 2011
Chat-IRES-Cre-neo	Uncategorized	Zeisel et al., 2018
Chrna2-Cre-OE25	Inhibitory	Leão et al., 2012
Cort-T2A-Cre	Inhibitory	Taniguchi et al., 2011
ctgf-T2A-dgCr	Excitatory	Tasic et al., 2016
Cux2-CreERT2	Excitatory	Zeisel et al., 2018
Drd3-Cre-KI196	Inhibitory	Volta et al., 2011
Efr3a-Cre-NO108	Uncategorized	Zeisel et al., 2018
Erbb4-T2A-CreERT2	Inhibitory	Madisen et al., 2010
Gabrr3-Cre-KC112	Inhibitory	Parolari 2020
Gad2-IRES-Cre	Inhibitory	Taniguchi et al., 2011
Gal-Cre-KI87	Excitatory	Zeisel et al., 2018
Grik4-Cre	Uncategorized	Zeisel et al., 2018
Htr2a-Cre-KM20	Excitatory	Rang et al., 2015
Lypd6-Cre-KL156	Uncategorized	Zeisel et al., 2018
Nos1-CreErt2	Inhibitory	Taniguchi et al., 2011
Npr3-IRES2-Cre	Excitatory	Daigle et al., 2018

Ntrk1-IRES-Cre	Uncategorized	Zeisel et al., 2018
Ntsr1-Cre-GN220	Excitatory	Madisen et al., 2010
Oxtr-Cre-ON66	Uncategorized	Zeisel et al., 2018
Oxtr-T2A-Cre	Uncategorized	
Pdzk1ip1-Cre-KD31	Uncategorized	Van der Togt et al., 1991
Plxnd-Cre-OG	Excitatory	Zeisel et al., 2018
Ppp1r17-Cre-NL1	Inhibitory	Zeisel et al., 2018
Prkcd-GluCla-CFP-IRES	Uncategorized	Zeisel et al., 2018
Pvalb-IRES-Cre	Inhibitory	Madisen et al., 2010
Rasgrf2-T2A-dCre	Uncategorized	Stacey et al., 2012
Rbp4-Cre-Kl100	Excitattory	Zeisel et al., 2018
Rorb-IRES-Cre	Uncategorized	Zeisel et al., 2018
Scnn1a-Tg3-Cre	Excitatory	Madisen et al., 2010
Sepw1-Cre-NP39	Uncategorized	Zeisel et al., 2018
Sim1-Cre-KJ18	Excitatory	Zeisel et al., 2018
Slc6a3-Cre	Uncategorized	Zeisel et al., 2018
Slc6a4-Cre-ET33	Uncategorized	Zeisel et al., 2018
Slc6a4-CreERT2-EZ13	Uncategorized	Zeisel et al., 2018
Slc6a5-Cre-KF10	Inhibitory	Morrow et al., 1998
Slc17a6-IRES-Cre	Excitatory	Harris et al., 2014
Slc17a8-IRES2-Cre	Excitatory	Tasic et al., 2018
Slc18a2-Cre-OZ14	Excitatory	Tritsch et al., 2014
Slc32a1-IRES-Cre	Inhibitory	Harris et al., 2014
Sst-IRES-Cre	Inhibitory	Taniguchi et al., 2011
Syt6-Cre-KI148	Uncategorized	Safran et al., 2010
Syt17-Cre-NO14	Excitatory	Ruhl et al., 2019
Tlx3-Cre-PL56	Excitatory	Cheng et al. 2004
Th-Cre-FI172	Uncategorized	Uhlèn et al., 2015

Supplemental Table 1: Type of neuron marked by each transgenic line

structure	wild type experiments	transgenic line experiments	transgenic lines	expressed in number of structures	transgenic line showing connections
MOp	8	21	15	13	12
ZI	4	15	13	11	11
PO	3	6	3	3	3
bfd	6	40	29	21	16
PSV	2	1	2	1	1
VTA	2	12	12	9	8
SI	7	10	8	7	7

SPVO	1	0	0	0	0
LC	0	0	0	0	0
SC	7	14	9	7	7
TM	0	1	1	0	0
VPM	3	6	6	5	5
VII	2	5	4	3	3
PPN	0	3	3	2	2
SPVC	3	6	6	5	5
SPVI	2	2	1	1	1
RT	2	11	7	7	7
DR	0	9	5	4	4

Supplemental Table 2: For each structure, this table presents the number of experiments ran (transgenic and wild), the number of transgenic lines tested, the number of transgenic lines showing marked neurons in the considered structures and the number of transgenic lines showing a connection.

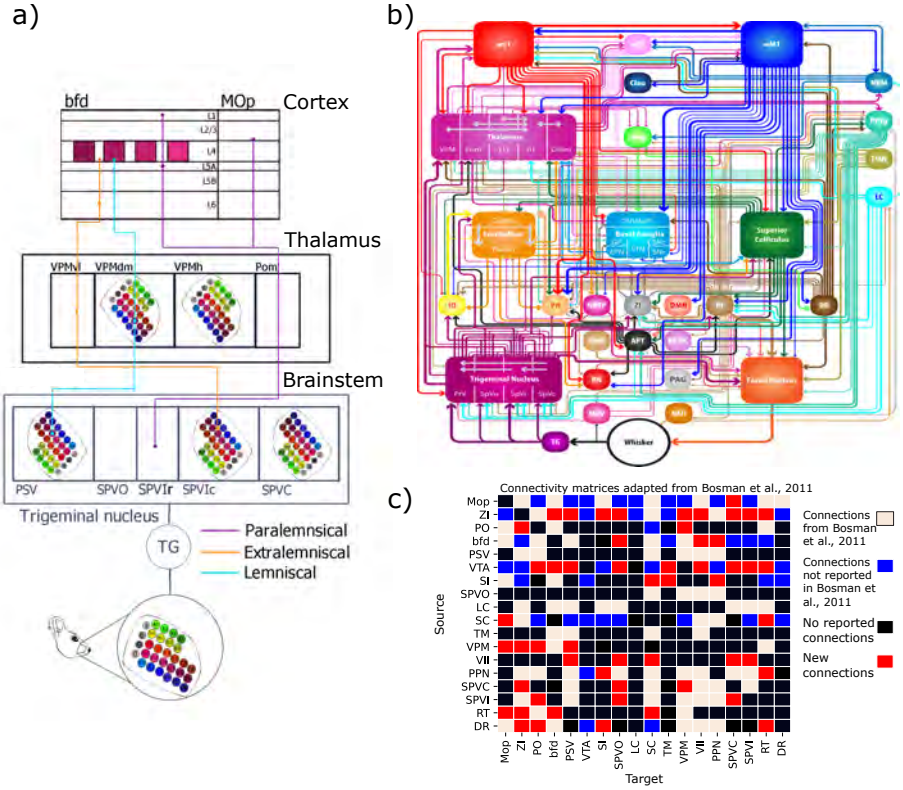

Supplemental Fig. 1 a) The whisker pad is organized in a grid-like structure. Each whisker is represented in SPVI, PSV, VPM, and bfd by an agglomerate of neurons organized in a barrel-like shape, respecting the coordinates of the whisker on the whisker pad with rotations. The information from the whisker enters the system through the trigeminal ganglion, projecting to the trigeminal nuclei. Here the information flow is divided into three major pathways: 1) the lemniscal pathway (blue), originating from the barrelettes of PSV, ascending to the barreloids of VPMdm and ending in the barrels of the layer 4 of the somatosensory pathway; 2) the extralemniscal pathway (orange), taking its origin in interbarrelette neurons of SPVI, connecting to VPMvl and targeting the primary somatosensory cortex; and 3) the paralemniscal pathway (purple), taking its source in SPVI, targeting PO, which then targets MOp and bfd. b) The connectivity map presented by Bosman et al. (2011).The 18 nuclei that we focus in our study present 72 connections in the previous map. c) The summary of the connections identified by Bosman and colleagues (color code: creme), experimentally identified connections since 2011 (blue), newly discovered anatomical projections identified in this work (red), and no known connections (black).

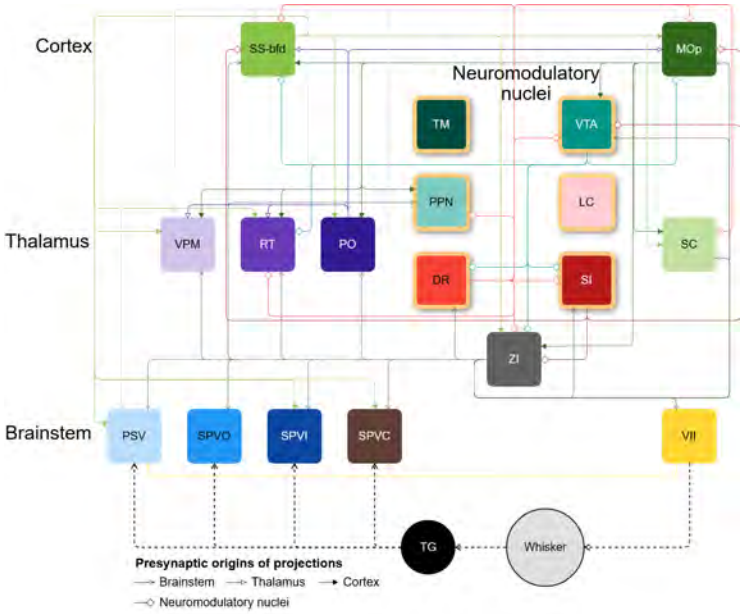

Supplemental Fig. 2 The excitatory connectivity map contains 61 connections. The dashed line represents the flow of information outside of the central nervous system. The neuromodulatory structures are represented with yellow borders.

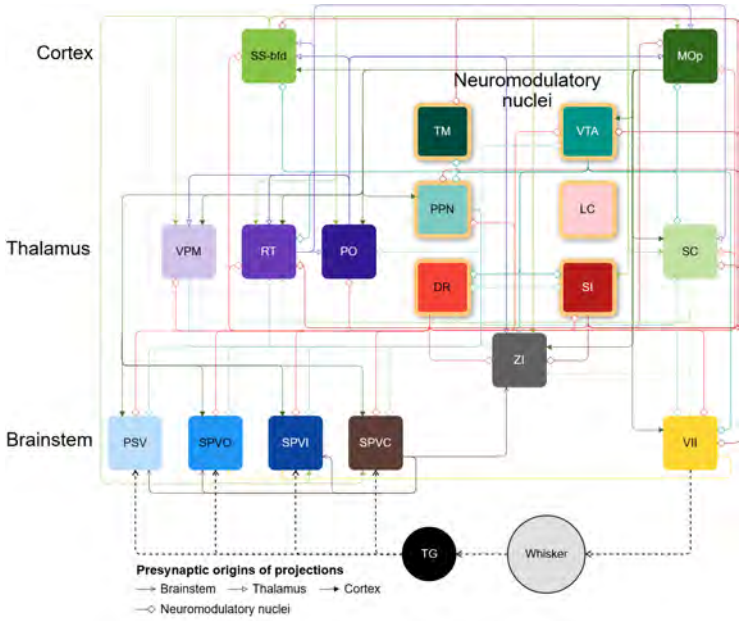

Supplemental Fig. 3 95 connections were revealed by uncategorized transgenic lines. The dashed line represents the flow of information outside of the central nervous system. The neuromodulatory structures are represented with yellow borders.

summary connections
source
target
Mop
ZI
PO
bfd
PSV
VTA
SI
SPVO
LC
SC
TM
VPM
VII
PPN
SPVC
SPVI
RT
DR
IP
FN
DN
CUL
PFL
AN
NOD
CENT
SIM
PYR
COPY
PRM
GRN
PRN
LRN
PARN
TRN
MOs
CLA
IO
APN
GP
XII
PAG
RN
STN
PB
LA
BLA
BMA
PA
CP
ACB
OT
LSc
LSr
LSv
CEA
MEA
Connection
No Connection

Supplemental Fig. 4 Summary of connection between 57 nuclei. **MOp**: Primary Motor Cortex, **Zi**: Zona Incerta, **PO**: Posterior complex of the thalamus, **bfd**: Barrel field of the primary somatosensory cortex, **PSV**: nucleus principalis of the trigeminal nucleus, **VTA**: Ventral tegmental area, **SI**: Substantia Innominata, **SPVO**: Spinal nucleus of the trigeminal nucleus oral part, **LC**: Locus coeruleus, **SC**: Superior Colliculus, **TM** : Tuberommaimillary Nucleus, **VPM**: Ventraposteromedial nucleus of the thalamus, **VII**: Facial motor nucleus, **PPN**: Pedunculopontine nucleus, **SPVC**: Spinal nucleus of the trigeminal nucleus caudal part, **SPVI**: Spinal nucleus of the trigeminal nucleus interoplaris part, **RT**: Reticular nucleus of the thalamus, **DR**: Dorsal Raphe nucleus, **IP**: Interposed nucleus, **FN**: Fastigial nucleus, **DN**: Dentate nucleus, **CUL**: Culmen, **PFL**: Paraflocculus, **AN**: Ansiform lobule, **NOD**: Nodulus(X), **CENT**: Central lobule, **SIM**: Simple lobule, **PYR**: Pyramus(VIII), **COPY**: Copula pyramidis, **PRM**: Paramedian lobule, **GRN**: Gigantocellular reticular nucleus, **PRN**: Pontine reticular nucleus, **LRN**: Lateral reticular nucleus, **PARN**: Parvicellular reticular nucleus, **TRN**: Tegmental reticular nucleus, **MOs**: Secondary motor area, **CLA** : Claustrum, **IO**: Inferior olivary complex, **APN**: Anterior pretectal nucleus, **GP**: Globus Pallidus, **XII**: Hypoglossal nucleus, **PAG**: Periaqueductal gray, **RN**: Red nucleus, **STN**: Subthalamic nucleus, **PB**: Parabrachial nucleus, **LA**: Lateral amygdalar nucleus, **BLA**: Basolateral amygdalar nucleus, **BMA**: Basomedial amygdalar nucleus, **PA**: Posterior amygdalar nucleus, **CP**: Caudoputamen, **ACB**: nucleus accumbens, **OT**: Olfactory tubercle, **LSc**: Lateral Septal nucleus caudal part, **LSr**: Lateral Septal nucleus rostral part, **LSv**: Lateral Septal nucleus ventral part, **CEA**: Central amygdalar nucleus, **MEA**: Medial amygdalar nucleus

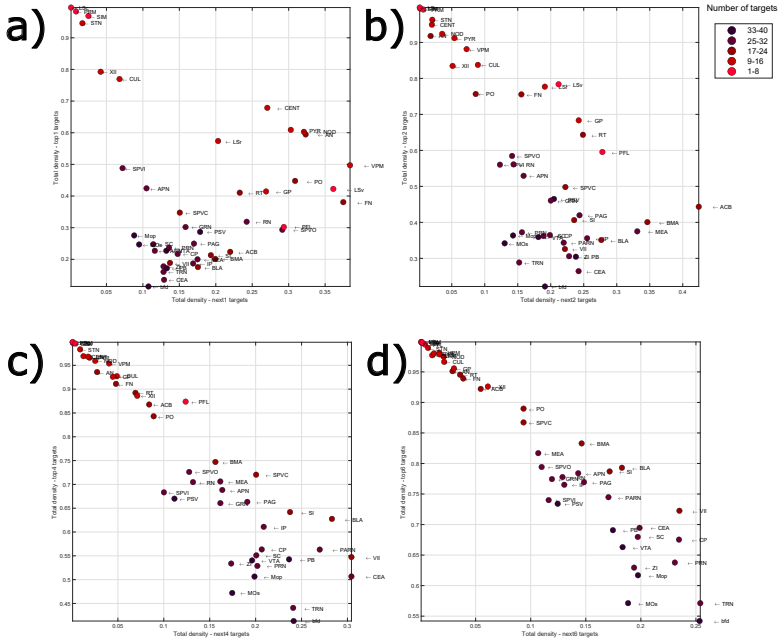

Supplemental Fig. 5 Cumulative density of incoming connections. Color scale represent the amount of out-degree per node. **a)** Comparison between the the percentage of incoming density explained by the densest connection and the second densest connection. **b)** Comparison between the the percentage of incoming density explained by the 2 densest connection and the next 2 densest connection. **c)** Comparison between the the percentage of incoming density explained by the 4 densest connection and the next 4 densest connection. **d)** Comparison between the the percentage of incoming density explained by the 6 densest connection and the next 6 densest connection.

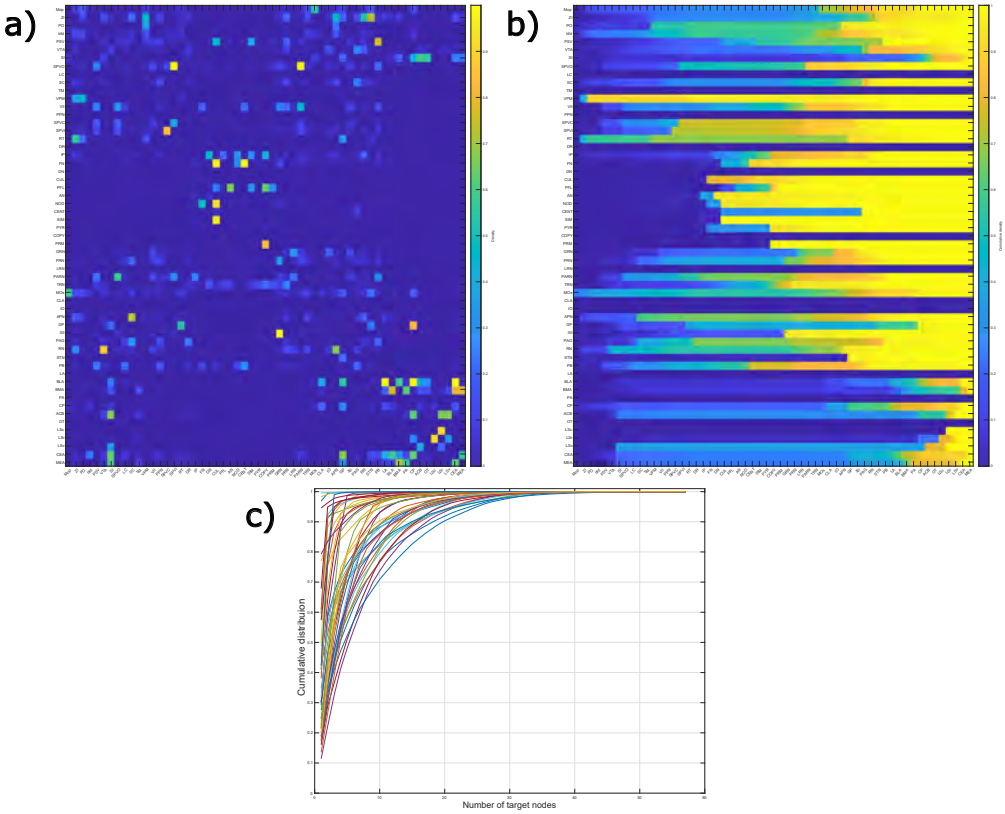

Supplemental Fig. 6 **a)** Connectivity matrix based on density of incoming connections and **b)** and **c)** cumulative density of incoming connections.

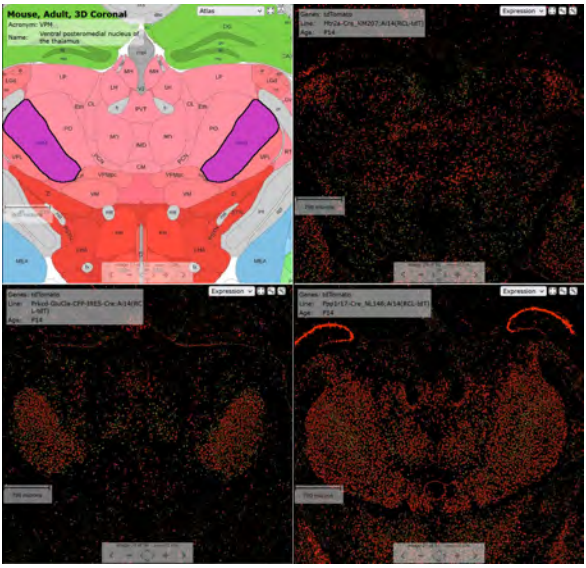

Supplemental Fig. 7 Expression in VPM of the transgenic lines PPP1r17 (inhibitory), Htr2a (Excitatory), and Prkcd (Uncategorized)

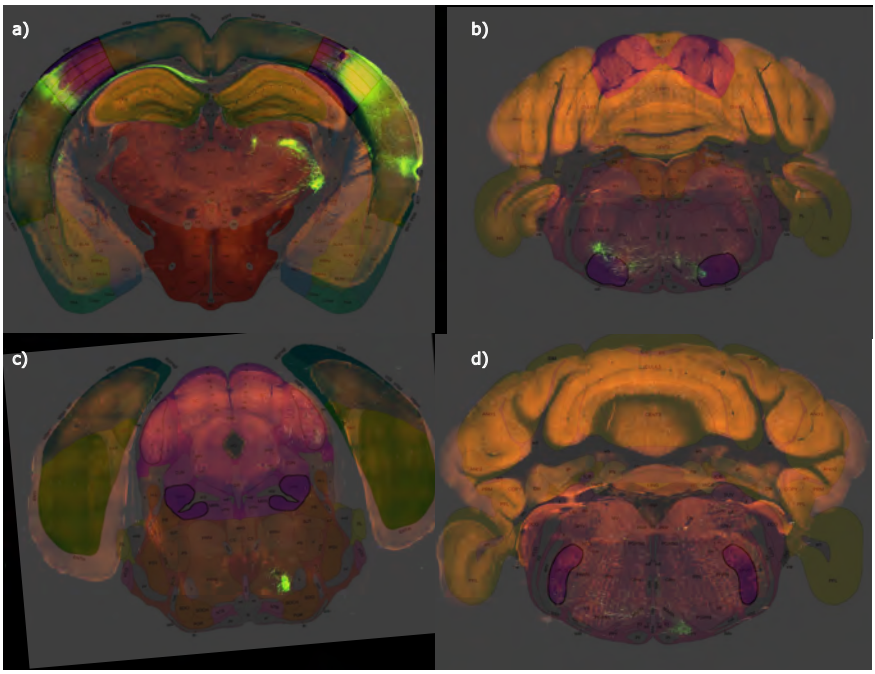

Supplemental Fig. 8 **a)** Injection structure bfd to **b)** VII, **c)** PPN, and **d)** SPVo. Experiment number 112951804, wild-type. The shortcomings of experimental procedures are addressed in the discussion.

Supplemental Fig. 9 **a)** Injection structure DR to **b)** SI. Experiment number 582609848, line Esr2-IRES2-Cre. The shortcomings of experimental procedures are addressed in the discussion.

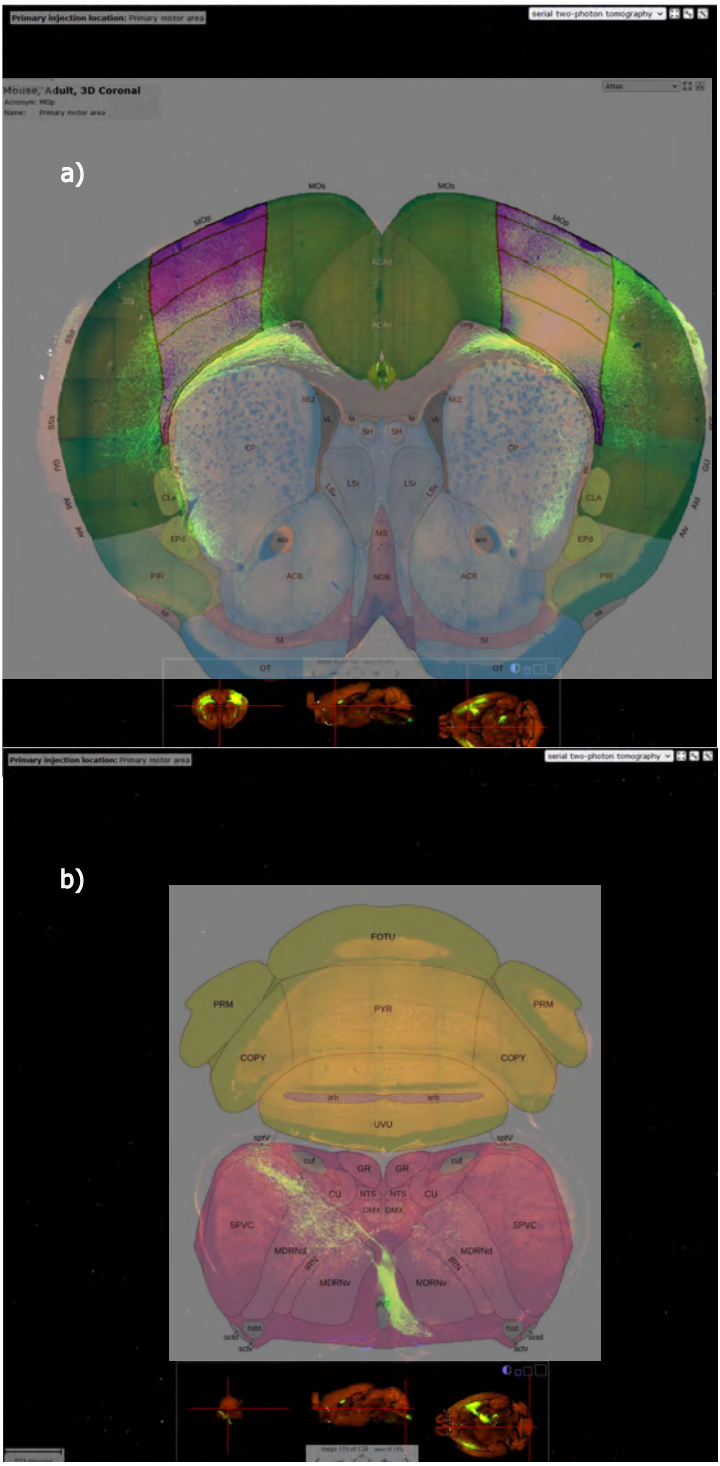

Supplemental Fig. 10 **a)** Injection structure MOp to **b)** SPVc. Experiment number 100141780, wild-type. The shortcomings of experimental procedures are addressed in the discussion.

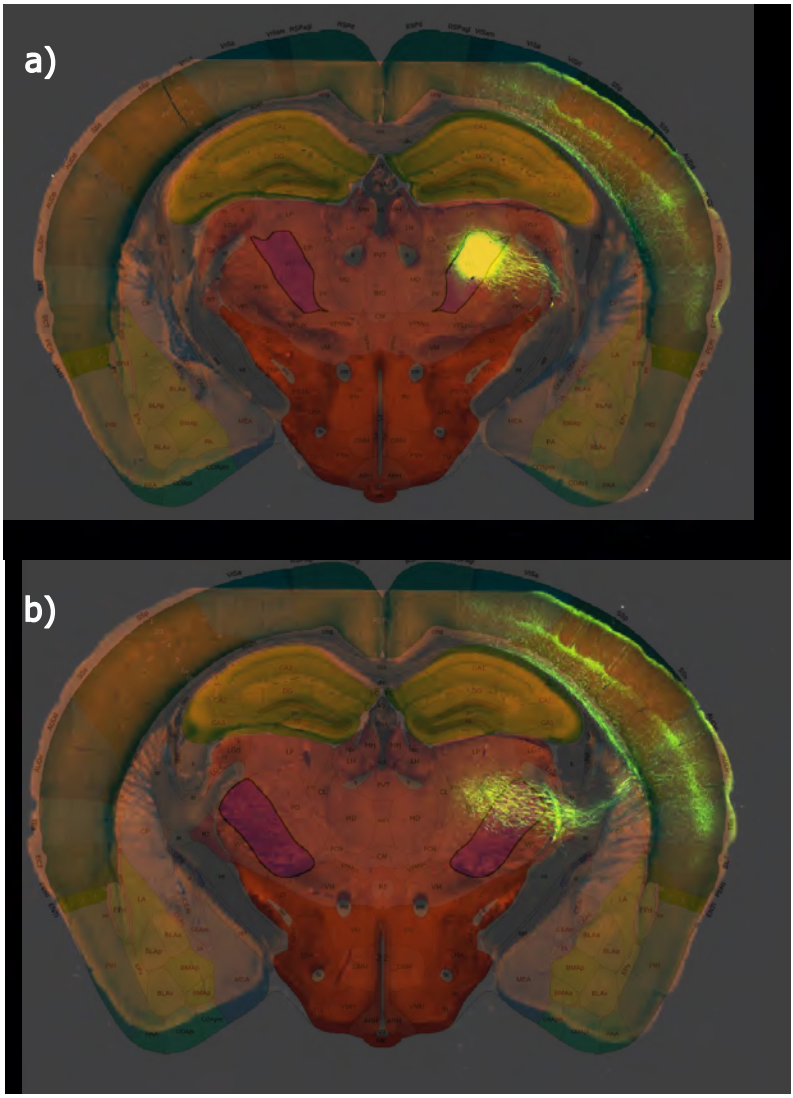

Supplemental Fig. 11 **a)** Injection structure PO to **b)** VPM. Experiment number 183011353, line Grik4-Cre. The shortcomings of experimental procedures are addressed in the discussion.

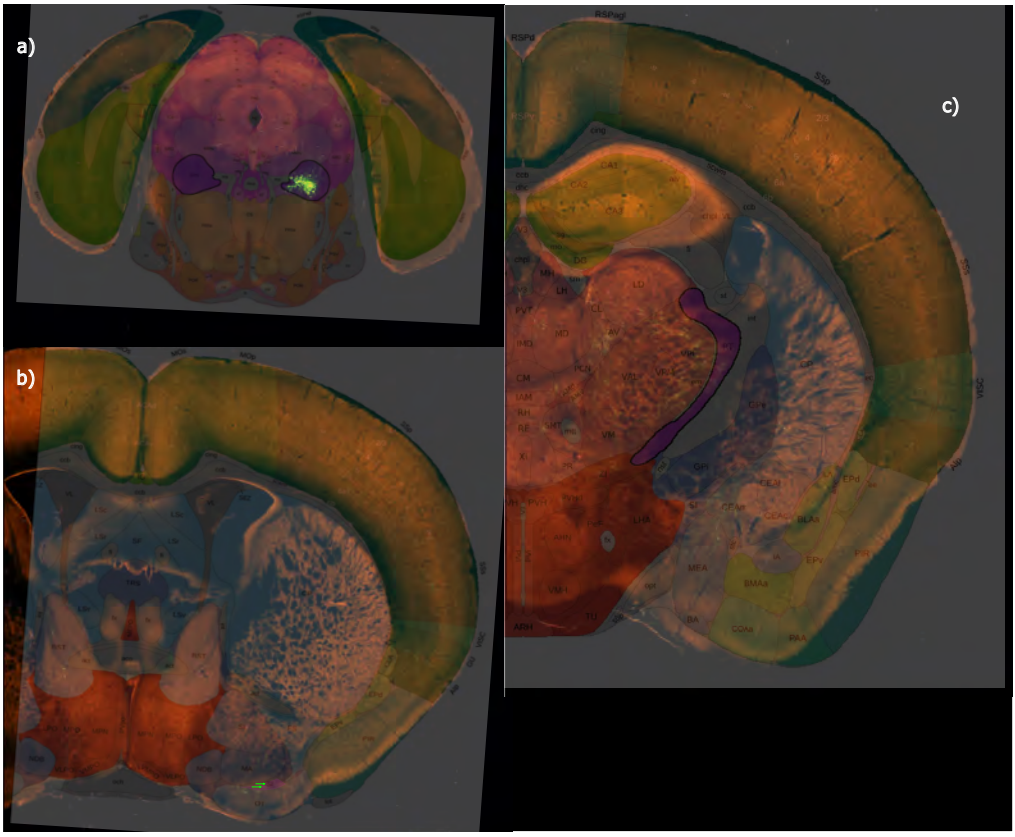

Supplemental Fig. 12 **a)** Injections structure PPN to **b)** SI and **c)** RT. Experiment number 264566672, line Chat-IRES-Cre-neo. The shortcomings of experimental procedures are addressed in the discussion.

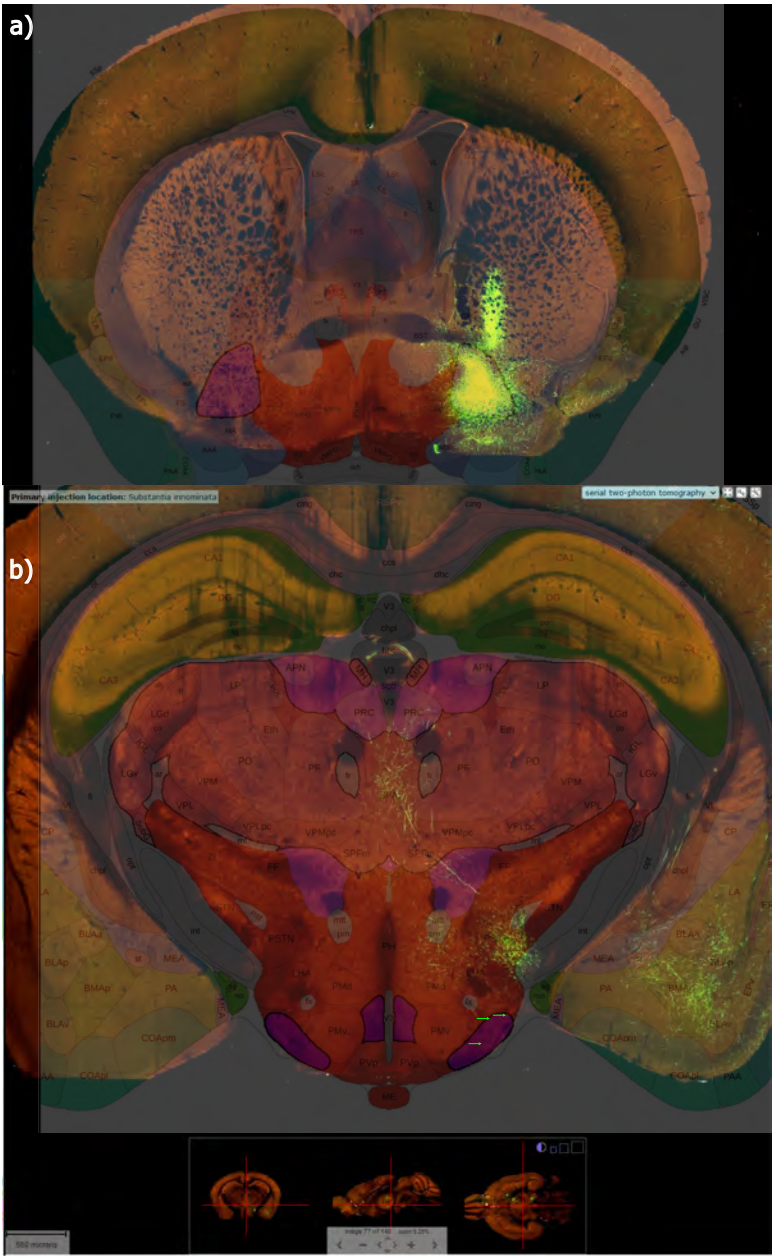

Supplemental Fig. 13 a) Injection structure SI to **b)** TM. Experiment number 305026861, line Drd3-Cre-KI196. The shortcomings of experimental procedures are addressed in the discussion.

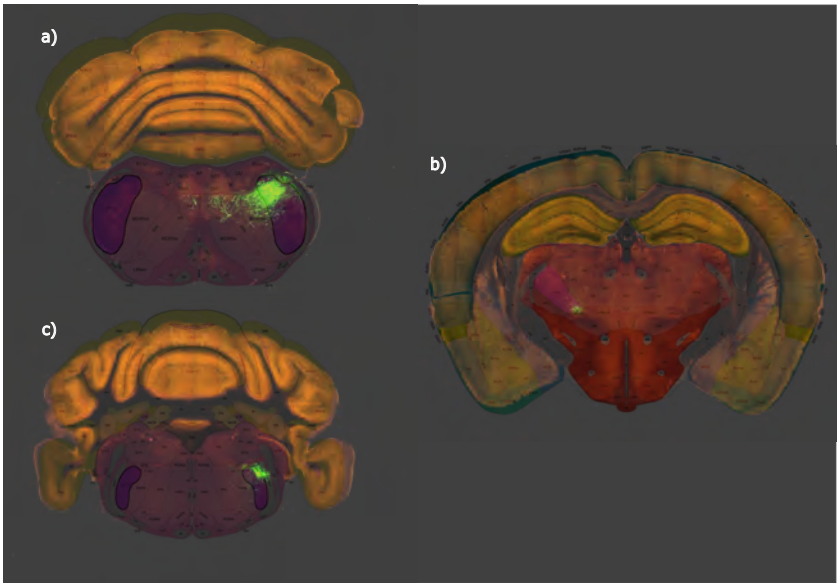

Supplemental Fig. 14 **a)** Injection structure SPVc to **b)** VPM and **c)** SPVo. Experiment number 114402050, wild-type. The shortcomings of experimental procedures are addressed in the discussion.

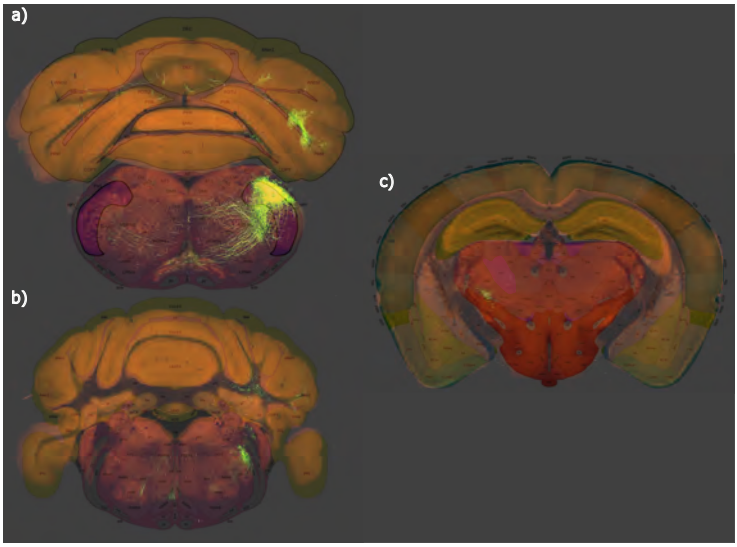

Supplemental Fig. 15 **a)** Injection structure SPVi to **b)** SPVo and **c)** PO. Experiment number 272738620, wild-type. The shortcomings of experimental procedures are addressed in the discussion.

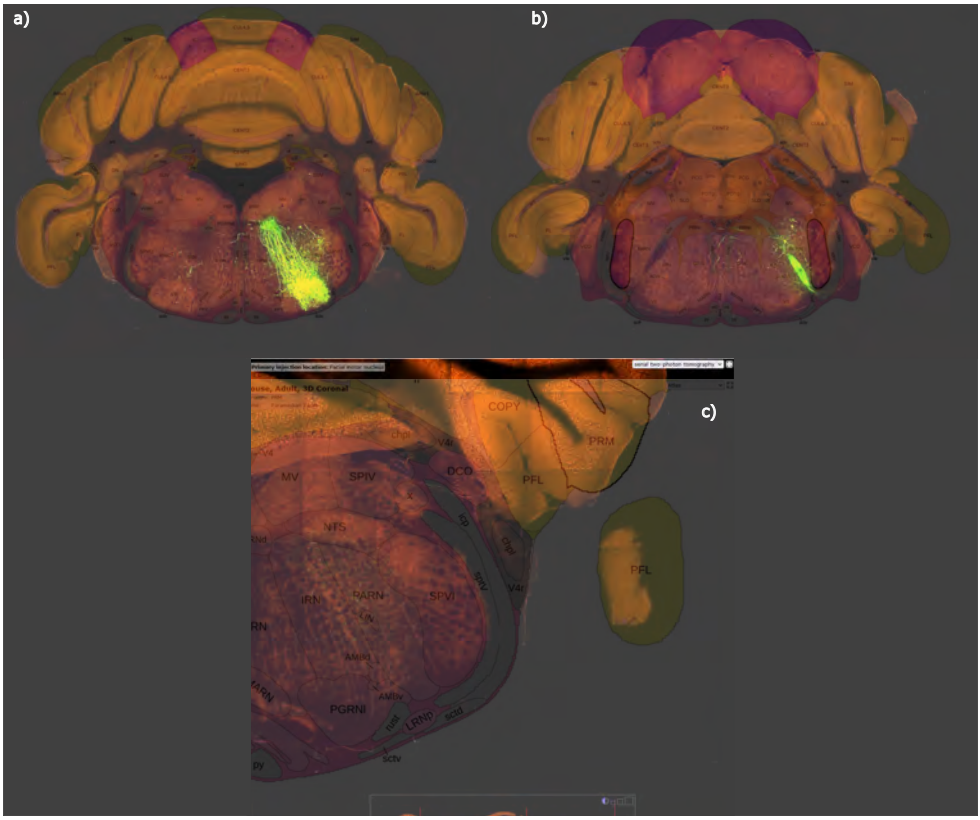

Supplemental Fig. 16 **a)** Injection structure VII to SPVo **b)** PSV, and **c)** to SPVi. Experiment number 177905562, line Scnn1a-Tg2-Cre. The shortcomings of experimental procedures are addressed in the discussion.

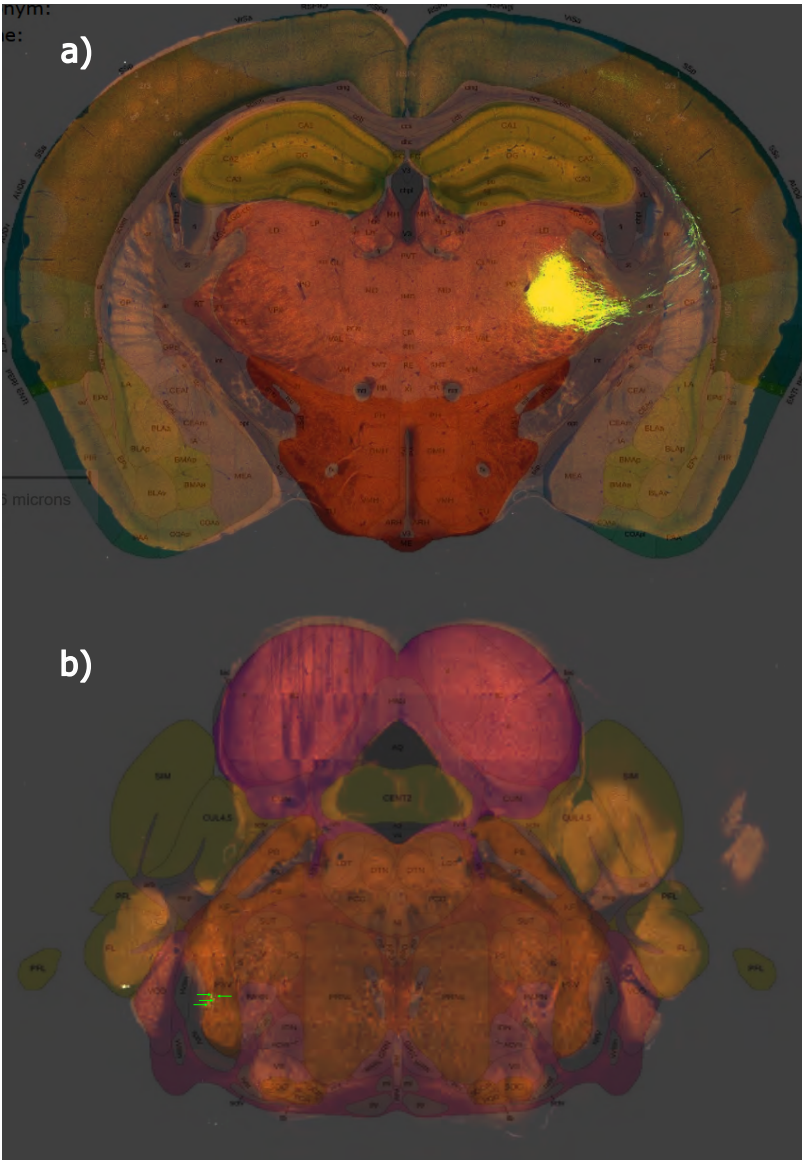

Supplemental Fig. 17 a) Injection structure VPM to **b)** PSV, experiment number 312240825, line Slc17a6-IRES-Cre. The shortcomings of experimental procedures are addressed in the discussion.

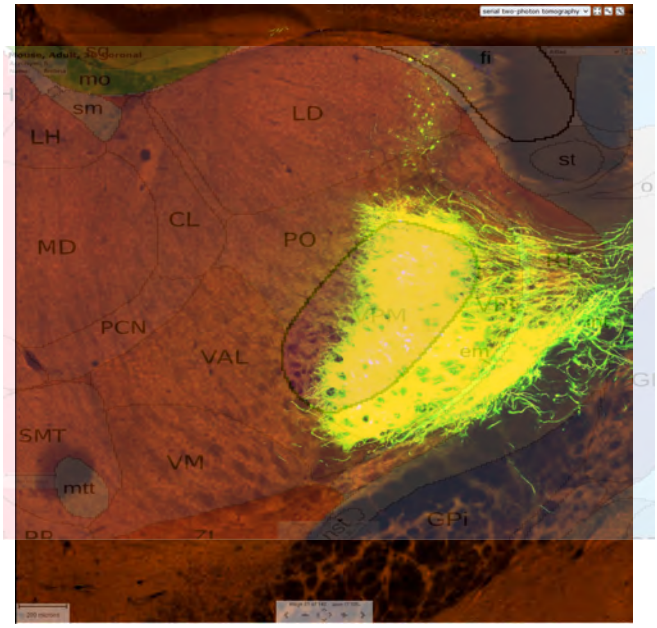

Supplemental Fig. 18 Inhibition target and source VPM to PO, experiment number 268206050, line Ppp1r17-Cre-NL146. The shortcomings of experimental procedures are addressed in the discussion.

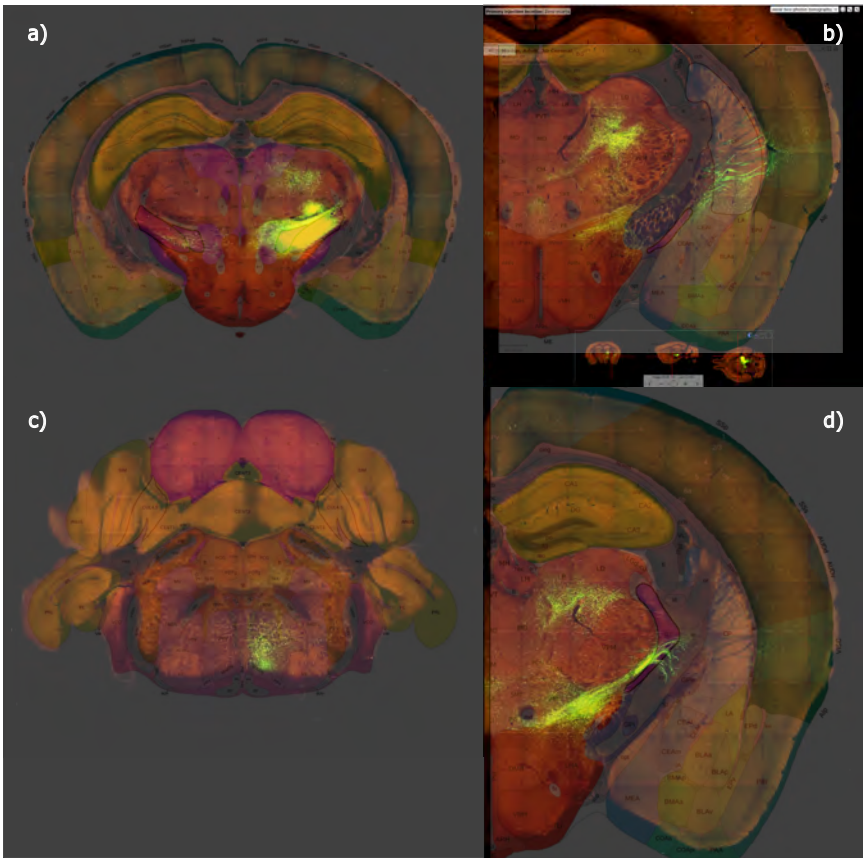

Supplemental Fig. 19 **a)** Injection structure ZI to **b)** SI, **c)** PSV, **d)** RT. Experiment number 113095845, wild-type. The shortcomings of experimental procedures are addressed in the discussion.

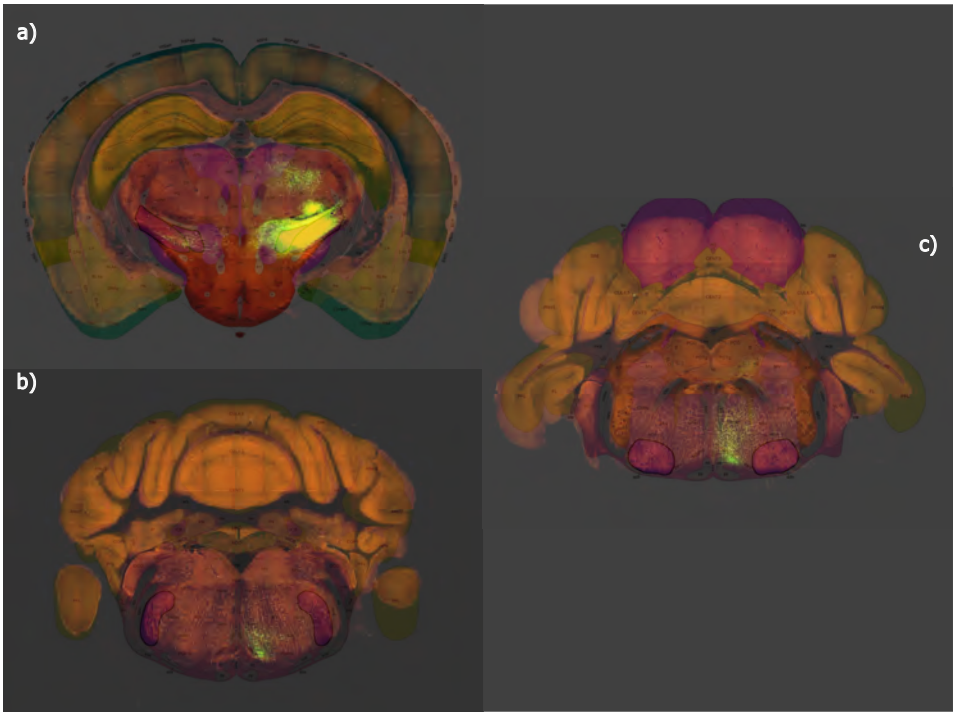

Supplemental Fig. 20 **a)** Injection structure ZI to **b)** SPVo, and **c)** VII. Experiment number 113095845, wild-type. The shortcomings of experimental procedures are addressed in the discussion.

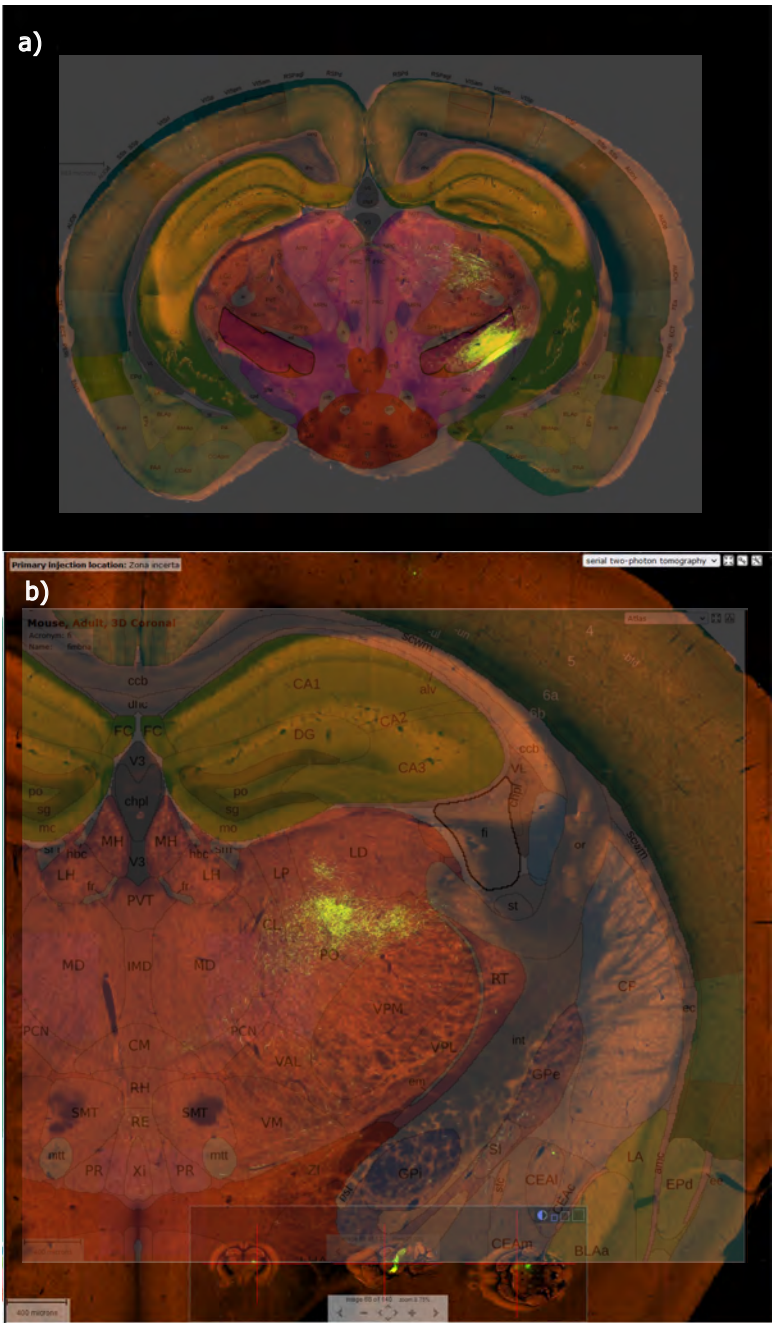

Supplemental Fig. 21 a) Injection structure ZI to **b)** VPM. Experiment number 301539438, line Pvalb-IRES-Cre. The shortcomings of experimental procedures are addressed in the discussion.